Cingulo-Opercular Control Network Supports Disused Motor Circuits in Standby Mode

Authors:
Dillan J. Newbold[1,*], Evan M. Gordon[2], Timothy O. Laumann[3], Nicole A. Seider[1], David F. Montez[1,3], Sarah J. Gross[1], Annie Zheng[1], Ashley N. Nielsen[1,4], Catherine R. Hoyt[5], Jacqueline M. Hampton[3], Mario Ortega[1], Babatunde Adeyemo[1], Derek B. Miller[1], Andrew N. Van[1,6], Scott Marek[1], Bradley L. Schlaggar[7,8,9], Alexandre R. Carter[1,5], Benjamin P. Kay[1], Deanna J. Greene[2,3], Marcus E. Raichle[1,2], Steven E. Petersen[1,2,6,10,11], Abraham Z. Snyder[1,2], Nico U.F. Dosenbach[1,2,5,6,12,*]

Affiliations:
[1]Department of Neurology, Washington University School of Medicine, St. Louis, MO 63110, USA.
[2]Department of Radiology, Washington University School of Medicine, St. Louis, MO 63110, USA.
[3]Department of Psychiatry, Washington University School of Medicine, St. Louis, MO 63110, USA.
[4]Institute for Innovations in Developmental Sciences, Northwestern University, Chicago, IL 60611, USA.
[5]Program in Occupational Therapy, Washington University School of Medicine, St. Louis, MO 63110, USA.
[6]Department of Biomedical Engineering, Washington University in St. Louis, St. Louis, MO 63110, USA.
[7]Kennedy Krieger Institute, Baltimore, MD 21205, USA.
[8]Department of Neurology, Johns Hopkins University School of Medicine, Baltimore, MD 21287, USA.
[9]Department of Pediatrics, Johns Hopkins University School of Medicine, Baltimore, MD 21287, USA.
[10]Department of Neuroscience, Washington University School of Medicine, St. Louis, MO 63110, USA.
[11]Department of Psychological and Brain Sciences, Washington University in St. Louis, St. Louis, MO 63110, USA.
[12]Department of Pediatrics, Washington University School of Medicine, St. Louis, MO 63110, USA.
*Correspondence: newbold@wustl.edu, dosenbachn@wustl.edu

Abstract

Whole-brain resting-state functional MRI (rs-fMRI) during two weeks of limb constraint revealed that disused motor regions became more strongly connected to the cingulo-opercular network (CON), an executive control network that includes regions of the dorsal anterior cingulate cortex (dACC) and insula (1). Disuse-driven increases in functional connectivity (FC) were specific to the CON and somatomotor networks and did not involve any other networks, such as the salience, frontoparietal, or default mode networks. Censoring and modeling analyses showed that FC increases during casting were mediated by large, spontaneous activity pulses that appeared in the disused motor regions and CON control regions. During limb constraint, disused motor circuits appear to enter a standby mode characterized by spontaneous activity pulses and strengthened connectivity to CON executive control regions.

Significance

Many studies have examined plasticity in the primary somatosensory and motor cortex during disuse, but little is known about how disuse impacts the brain outside of primary cortical areas. We leveraged the whole-brain coverage of resting-state functional MRI (rs-fMRI) to discover that disuse drives plasticity of distant executive control regions in the cingulo-opercular network (CON). Two complementary analyses, pulse censoring and pulse addition, demonstrated that increased functional connectivity between the CON and disused motor regions was driven by large, spontaneous pulses of activity in the CON and disused motor regions. These results point to a previously unknown role for the CON in supporting motor plasticity and reveal spontaneous activity pulses as a novel mechanism for reorganizing the brain's functional connections.

Introduction

Disuse is a powerful paradigm for inducing plasticity that has uncovered key organizing principles of the human brain (2-5). Monocular deprivation revealed that multiple afferent inputs can compete for representational territory in the primary visual cortex (2). Competition between afferents also shapes the somatomotor system, and manipulations such as peripheral nerve deafferentation, whisker trimming, and limb constraint all drive plasticity in the primary somatosensory and motor cortex (3-5). Most plasticity studies to date have used focal techniques, such as microelectrode recordings, to study local changes in brain function. As a result, little is known about how behavior and experience shape the brain-wide functional networks that support complex cognitive operations (6).

The brain is composed of networks of regions that cooperate to perform specific cognitive operations (6-9). These functional networks show synchronized spontaneous activity while the brain is at rest, a phenomenon known as resting state functional connectivity (FC) (10-12). FC can be measured non-invasively in humans using resting-state functional MRI (rs-fMRI). Whole-brain rs-fMRI has been used to parse the brain into canonical functional networks (13, 14), including visual, auditory and somatomotor networks (15, 16); ventral and dorsal attention networks (9, 17); a default mode network with roles in internally directed cognition and episodic memory (8, 12); a salience network thought to assess the homeostatic relevance of external stimuli (18); a frontoparietal control network supporting error-processing and moment-to-moment adjustments in behavior (1, 19, 20); and a cingulo-opercular control network (CON), which maintains executive control during goal-directed behavior (1, 19, 21).

A more recent advance in human neuroscience has been the recognition of individual variability in network organization (22-25). Most early rs-fMRI studies examined central tendencies in network organization using group-averaged FC measurements (11, 13, 14). Recent work has demonstrated that functional networks can be described in an individual-specific manner if sufficient rs-fMRI data are acquired, an approach termed Precision Functional Mapping (PFM) (22, 23, 26-30). PFM respects the unique functional anatomy of each person and avoids averaging together functionally distinct brain regions across individuals.

Somatomotor circuits do not function in isolation. Action selection and motor control are thought to be governed by complex interactions between the somatomotor network and control networks, including the CON (1). Here, we leveraged the whole-brain coverage of rs-fMRI and the statistical power of PFM to examine disuse-driven plasticity throughout the human brain.

Results

Disuse Caused Both Increases and Decreases in Functional Connectivity

Three adult participants ("Cast1", "Cast2" and "Cast3") were scanned at the same time every day for 42-64 consecutive days (30 minutes of rs-fMRI/day) before, during and after two weeks of dominant upper extremity casting (31). To examine disuse-driven plasticity beyond somatomotor networks, we first generated seed maps showing FC between L-$SM1_{ue}$ and all other cortical regions before, during and after casting (Fig. 1*A*, S1). Prior to casting (Pre), L-$SM1_{ue}$ was strongly connected to the remainder of the somatomotor cortex (pre- and post-central gyri), especially homotopic R-$SM1_{ue}$. During the cast period (Cast), L-$SM1_{ue}$ showed a new pattern of connectivity, with strong connections to bilateral secondary somatosensory cortex (SII), dorsal anterior cingulate cortex (dACC), and pre- and post-central sulci. After casting (Post), L-$SM1_{ue}$ FC returned to baseline. Changes in FC during casting (Cast – Pre) and recovery (Post – Cast) were examined using sets of previously published individual-specific cortical parcels (22, 31). Casting caused decreased L-$SM1_{ue}$ connectivity with the remainder of the somatomotor cortex, as well as increased connectivity with the bilateral SII, dACC, and pre- and post-central sulci (Fig. 1*B*, S1). FC changes after cast removal were strongly negatively correlated with changes during casting (Cast1: spatial correlation, $r = -0.56$, Cast2: $r = -0.95$, Cast3: $r = -0.32$; all participants: $P < 0.001$), indicating that most effects reversed after cast removal (Fig. 1*B*, S1).

Disuse-driven Functional Connectivity Changes Were Highly Focal in Network Space

The brain's functional network organization can be visualized using spring-embedded graphs, which treat functional connections as spring forces, positioning more strongly connected nodes closer to one another (Fig. 2*A*, S2). While L-$SM1_{ue}$ FC increases were distributed in anatomical space, including regions on the medial and lateral surfaces of both hemispheres, nearly all of

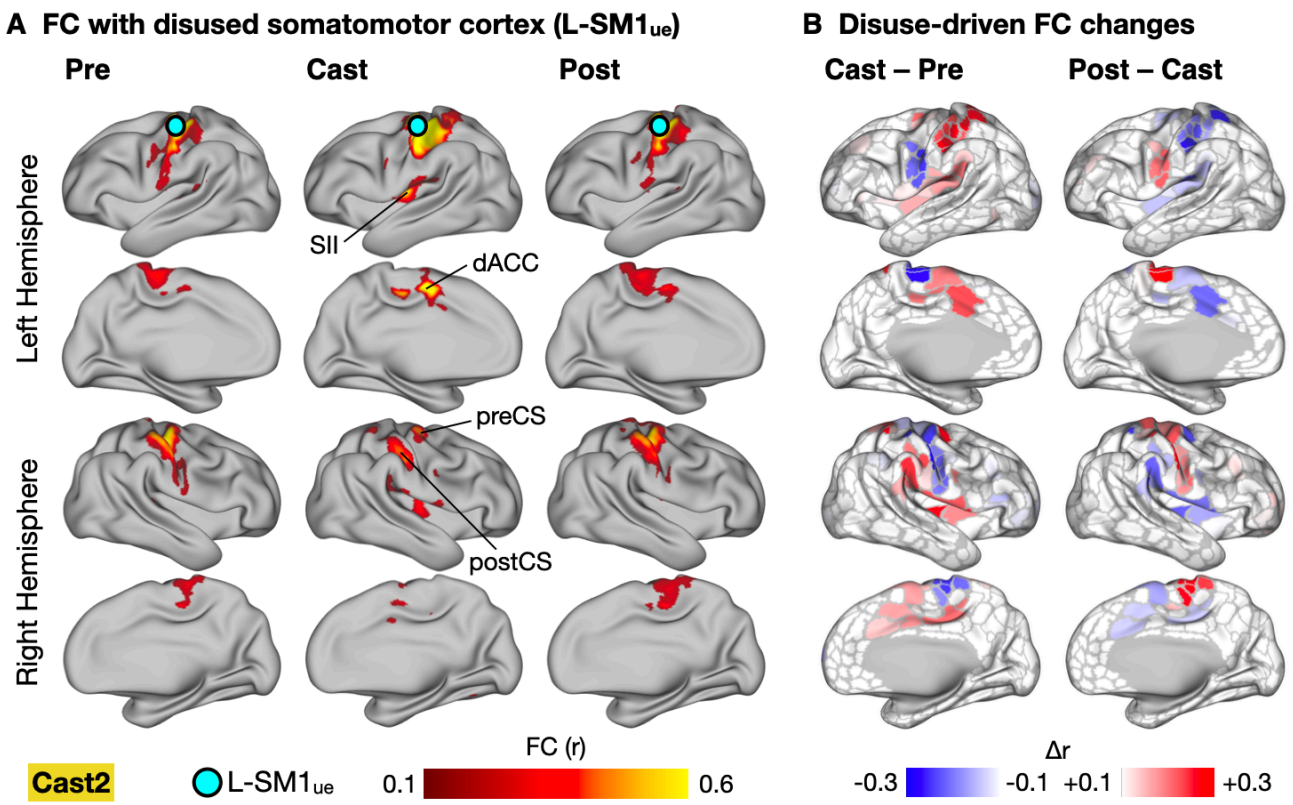

Fig. 1. Cast-driven Changes in Functional Connectivity (FC) of Disused Somatomotor Cortex (L-SM1$_{ue}$). (A) Seed maps showing FC between L-SM1$_{ue}$ and the remainder of the cerebral cortex in an example participant (Cast2; remaining participants, Fig. S1). Seed maps were averaged across sessions before, during and after casting (Pre, Cast, Post). Labels indicate secondary somatosensory cortex (SII), dorsal anterior cingulate cortex (dACC), and pre- and post-central sulci (preCS and postCS). (B) Subtraction maps showing changes in FC during casting (Cast – Pre) and recovery (Post – Cast). Differences are shown on a set of previously published individual-specific cortical parcels (22, 31).

these changes mapped onto a single cluster in network space, the CON (Fig. 2*B*, S2). The network focality of L-SM1$_{ue}$ FC increases was quantified by examining the distribution of the greatest FC increases (top 5%) across the canonical functional networks (Fig. 2*B*). In all participants, the CON showed more FC increases than expected by chance ($P < 0.001$ for all participants). Decreases in L-SM1$_{ue}$ FC were also localized in network space (Fig. 2*C*, S2). Most of the regions showing decreased FC with L-SM1$_{ue}$ during casting belonged to the somatomotor networks (ue-SMN, le-SMN, face-SMN and premotor). All participants showed more FC decreases than expected by chance in the upper-extremity somatomotor network (ue-SMN; $P < 0.001$ for all participants). Additionally, two participants (Cast2 and Cast3)

showed significant FC decreases in other somatomotor networks, including the lower-extremity and face somatomotor networks (le-SMN and f-SMN) and the premotor network.

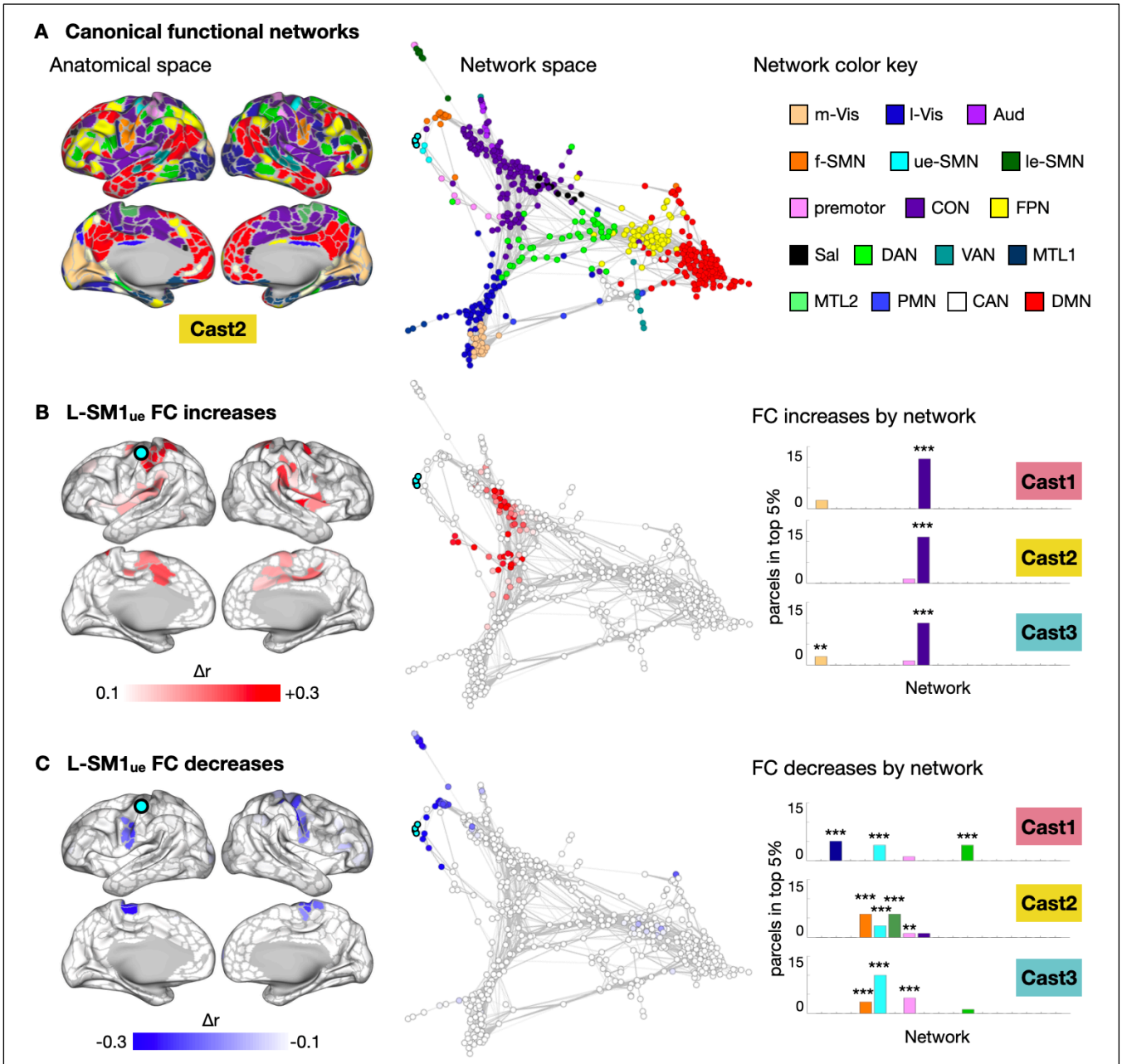

Fig. 2, Disused Somatomotor Cortex (L-SM1$_{ue}$) Functional Connectivity (FC) Changes in Network Space. (A) Map of canonical functional networks in an example participant (Cast2; remaining participants, Fig. S1). *Left:* Networks shown in anatomical space (inflated cortical surfaces). *Middle:* Same map as *Top*, shown in network space (spring-embedded graphs based on Pre scans). *Right:* Network color key: m-Vis: medial visual; l-Vis: lateral visual; Aud: auditory; f-SMN: face somatomotor; ue-SMN: upper-extremity somatomotor; le-SMN: lower-extremity somatomotor; CON: cingulo-opercular; FPN: fronto-parietal; Sal: salience; DAN: dorsal attention; VAN: ventral attention; MTL: medial temporal lobe; PMN: parietal memory; CAN: context association; DMN: default mode. (B) *Left:* Subtraction maps showing disuse-driven decreases in functional connectivity (FC) with left somatomotor cortex (L-SM1$_{ue}$) in anatomical space. *Middle:* Same map as *Top,* shown in network space. *Right:* Distribution of top 5% FC decreases across all networks. **P < 0.01; ***P < 0.001; FDR < 0.05. (C) Subtraction maps showing disuse-driven increases in FC with L-SM1$_{ue}$ in anatomical (*Left*) and network space (*Middle*). *Right:* Distribution of top 5% FC increases across all networks.

Plasticity Was Restricted to the Somatomotor and Cingulo-opercular Networks

The analyses presented thus far focus on changes in connectivity between L-SM1$_{ue}$ and the remainder of the cerebral cortex. To examine whole-brain patterns of FC changes induced by casting, we extracted rs-fMRI signals from individual-specific cortical, subcortical and cerebellar parcels (Cast1: 744 parcels, Cast2: 733; Cast3: 761) and examined FC changes in all possible pairwise connections (Fig. S3). We displayed the 50 largest changes in FC (25 greatest increases and 25 greatest decreases) in anatomical space (Fig. 3*A*, S3). Disuse-driven FC changes involved L-SM1$_{ue}$ more than expected by chance (Cast1: 9/50 connections, P = 0.018; Cast2: 37/50, P < 0.001; Cast3: 39/50, P < 0.001). Figure 3*B* shows the total

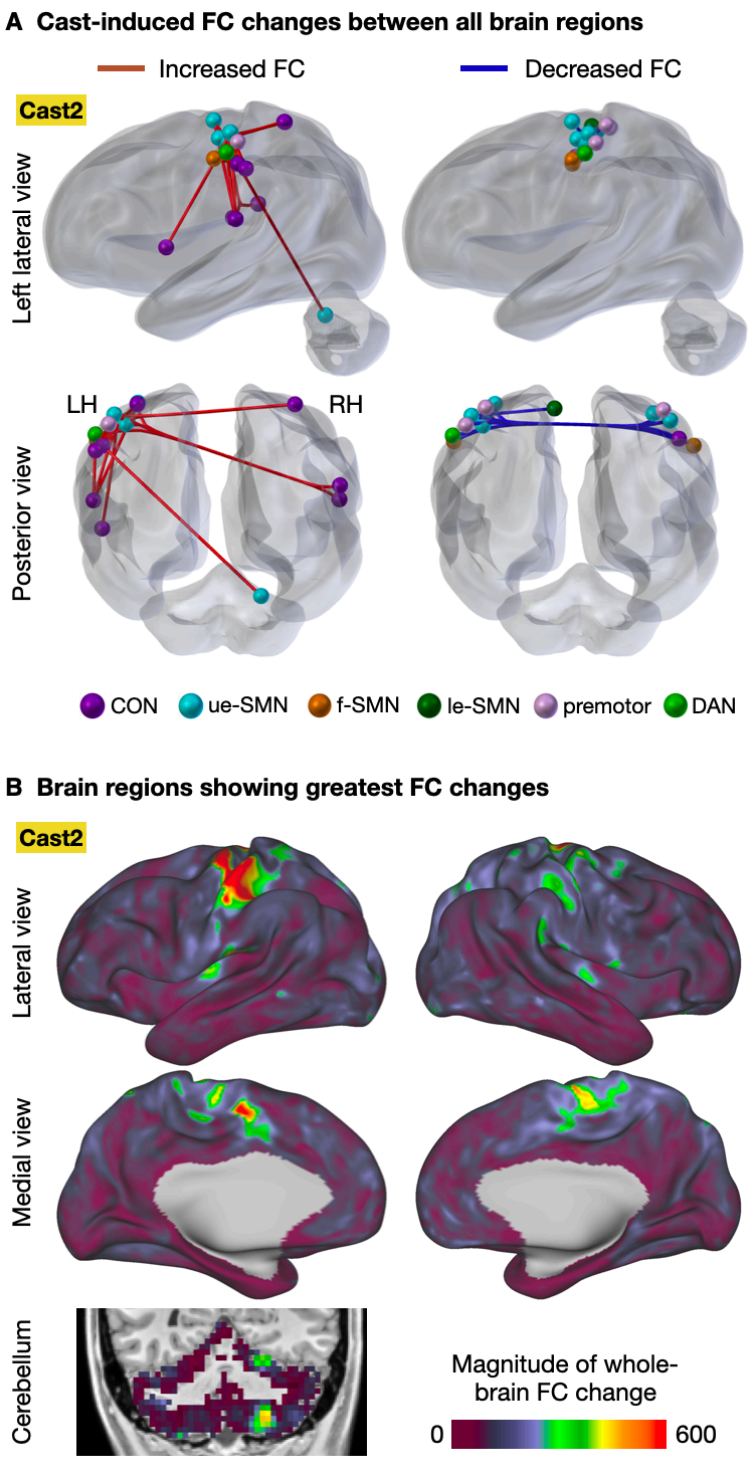

Fig. 3. Whole-brain Analyses of Disuse-driven Functional Connectivity (FC) Changes. (A) Changes in functional connectivity (FC) were computed for all pairs of cortical, subcortical and cerebellar parcels (mean Cast FC – mean Pre FC). The 50 most altered functional connections (top 25 increases, top 25 decreases) are shown for an example participant (Cast2; all participants, Fig. S3). (B) For each vertex/voxel, the magnitude of whole-brain FC change was computed as the sum of squared FC changes between that vertex and every other gray-matter vertex/voxel. Shown for an example participant (Cast2; all participants shown in Fig. S4).

magnitude of whole-brain FC change for each vertex/voxel. The total magnitude of whole-brain FC change was significantly greater in L-SM1$_{ue}$ than in the remainder of the brain (Fig. 3*B*, S3; Cast1: P = 0.021; Cast2: P < 0.001; Cast3: P = 0.005).

Increased Connectivity with the CON Depended on a Recent History of Disuse

To distinguish between increases in connectivity due to wearing a cast during MRI scans (i.e., an altered behavioral state) and increases in connectivity due to a history of having been casted (i.e., disuse-driven plasticity), we conducted a control experiment in which participants wore casts during 30-minute scans but were not casted during their daily lives. In both cases, we compared FC between L-SM1$_{ue}$ and the left dorsal anterior cingulate cortex (L-dACC; Fig. S4*A*), a key node of the CON, in cast and no-cast conditions. As suggested by the whole-brain network analyses (Fig. 2*B*), FC between L-SM1$_{ue}$ and L-dACC was significantly increased during the cast period (Fig. S4*B*). When participants wore casts during scans, but were not casted during their daily lives, no changes in FC were observed (Fig. S4*C*). This control experiment indicated that increased FC between the disused motor circuitry and the CON depended on participants' recent history of disuse, not their current state of casting.

Network-Specific Connectivity Changes Reflect Spontaneous Activity Pulses

Increases in FC with L-SM1$_{ue}$ showed a similar anatomical distribution to the spontaneous activity pulses we described previously (31) (Fig. S5*A*-*B*). Additionally, FC between L-SM1$_{ue}$ and the CON was highly correlated with the number of pulses detected in L-SM1$_{ue}$ during each scan (Fig. S5*C*; Cast1: r=0.74, Cast2: r=0.57, Cast3: r=0.73; all participants: P<0.001). These observations led us to suspect that FC between L-SM1$_{ue}$ and the CON was increased during the cast period because both regions showed synchronized spontaneous activity pulses.

To test if spontaneous activity pulses could explain observed increases in FC, we implemented a pulse censoring strategy, in which frames surrounding each detected pulse (13.2 s before – 17.6 s after each pulse peak) were excluded from FC calculations (Fig. 4*A*). This approach is similar to the censoring strategy commonly used to correct the effects of head-motion on FC (32). Censoring pulses partially reduced the FC changes observed during casting (Fig. 4*B*; Cast1 -55%, P = 0.14; Cast2: -28%, P = 0.02; Cast3: -21%, P = 0.04; one-tailed t-test). Additionally, the spatial pattern of FC changes caused by pulse censoring (Censored – Uncensored; Fig. 4*C*, S6) was negatively correlated with FC changes during casting (Cast1: r = -0.35, Cast2: r = -0.90, Cast3: r = -33; all participants: P < 0.001).

Censoring pulses did not entirely eliminate the effect of casting on FC. The residual effect of casting after pulse censoring was negatively spatially correlated with the effects of pulse censoring (Fig. S6; Cast1: spatial correlation, r = -0.23, Cast2: r = -0.76, Cast3: r = -0.18; all participants: P < 0.001), suggesting that the residual effect may have been driven by

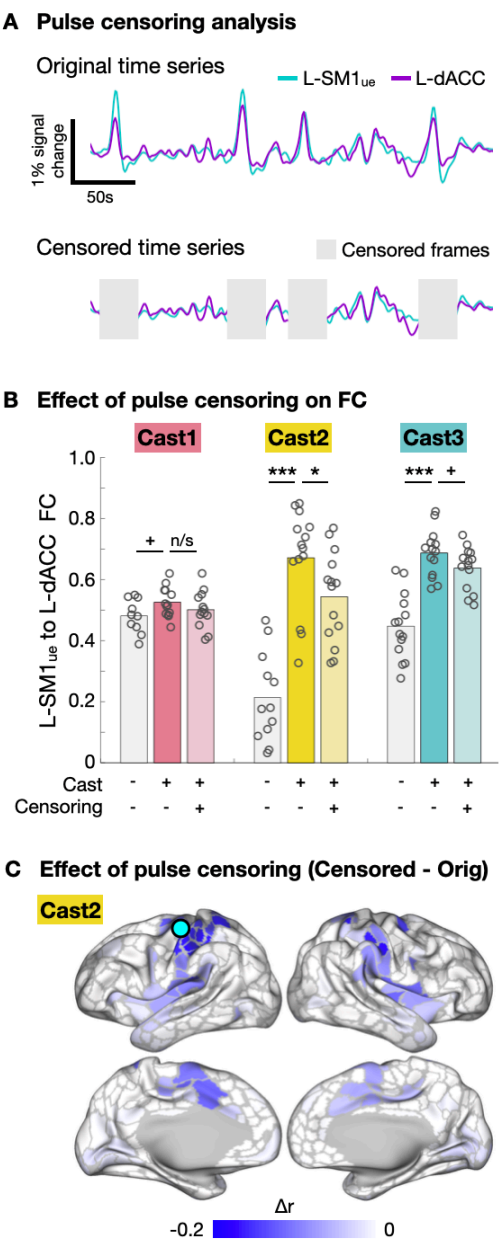

Fig. 4. Censoring Pulses from Functional Connectivity (FC) Measurements. (A) Schematic explaining censoring approach used to remove detected pulses from FC calculation. (B) Censoring pulses partially reduced the difference between Pre and Cast scans. $^{+}$P < 0.1, *P < 0.05, ***P < 0.001. (C) Subtraction map showing reductions in L-SM1$_{ue}$ FC due to pulse censoring. The spatial pattern of FC changes due to pulse censoring was significantly negatively correlated with FC changes during casting (Cast1: r = -0.35, Cast2: r = -0.90, Cast3: r = -0.33; all participants: P < 0.001)

additional pulses that were too small to distinguish from ongoing spontaneous activity fluctuation. Pulses showed a wide distribution of magnitudes (Fig. 5*A*; range: 0.4 – 1.2% rs-fMRI signal change). Because pulses were detected using a threshold-based approach (31), pulses smaller than 0.4% fMRI signal change could not be detected and censored. To test if smaller pulses that escaped detection could explain the residual increased FC between L-SM1$_{ue}$ and L-dACC after pulse censoring, we simulated a full distribution of pulse magnitudes by adding the mean pulse time series from L-SM1$_{ue}$ and L-dACC to the baseline rs-fMRI signals recorded from these regions prior to casting (Fig. 5*B*). Simulated pulse magnitudes were drawn from a log-normal distribution, fit to the magnitude distribution of detected pulses using a least-squares approach (Fig. 5*A*; see S7 for triangular and exponential distributions). Adding simulated pulses caused FC increases with a similar effect size (Cast1: $\Delta r = +0.07$, $P = 0.013$; Cast2: +0.40, $P < 0.001$; Cast3: +0.19, $P < 0.001$) to the FC increases observed during

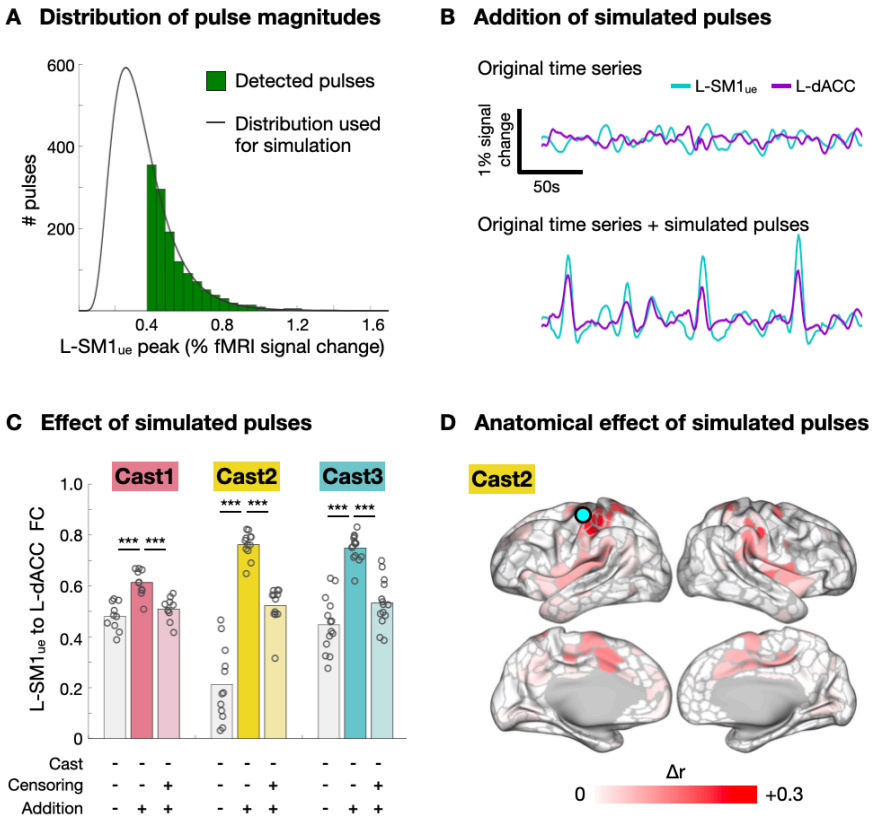

Fig. 5. Addition of Simulated Pulses. (A) Histogram of pulse magnitudes (peak fMRI signal), pooled across participants. A log-normal distribution (black line) was fit to the data using a least-squares approach. (B) *Top:* Example resting-state functional MRI (rs-fMRI) signals from disused motor cortex (L-SM1$_{ue}$) and the dorsal anterior cingulate cortex (L-dACC) recorded prior to casting (Pre). *Bottom:* Same time series with simulated pulses added at random time points. Simulated pulse magnitudes were drawn from the full distribution shown in panel A. (C) Adding simulated pulses increased FC between L-SM1$_{ue}$ and L-dACC (***P<0.001). Censoring simulated pulses partially reduced FC increases (***P<0.001). (D) Subtraction map showing increases in L-SM1$_{ue}$ FC caused by simulated pulses in an example participant (Cast2; all participants, Fig. S7).

194 casting (Fig. 5*C*). Applying the same pulse censoring strategy described above to the
195 simulated pulses partially reduced the increases in FC (Fig. 5*C*; Cast1: -79%, Cast2: -58%,
196 Cast3: -69%; all participants: $P < 0.001$), similar to the effect of pulse censoring on the actual
197 data (Fig. 4*B*). Adding simulated pulses to all brain regions, using mean pulse time series
198 specific to each region, recreated the anatomical distribution of FC changes observed during
199 casting (Fig. 5*D*, S8; Cast1: $r = 0.44$, Cast2: $r = 0.95$, Cast3: $r = 0.64$; all participants: $P <$
200 0.001). Thus, pulse with a full distribution of magnitudes could account for observed FC
201 changes during casting and the partial reversal of FC changes after pulse censoring.
202
203 We also utilized the pulse censoring and pulse addition analyses to test if pulses could explain
204 observed decreases in FC within the somatomotor system. Pulse censoring did not
205 significantly reverse the decrease in FC between L-$SM1_{ue}$ and R-$SM1_{ue}$ observed during the
206 cast period (Fig. S9). Adding simulated pulses to baseline time series decreased FC between
207 L-$SM1_{ue}$ and R-$SM1_{ue}$, but this effect was much smaller than that observed during casting (Fig.
208 S9).
209

210 ## Discussion

211 **Disuse Drives Plasticity of Functional Networks**

212 Daily 30-minute scans of rs-fMRI before, during, and after casting revealed that disuse not only
213 causes plasticity within the primary motor cortex (4, 31), but also increased functional
214 connectivity between disused circuits and executive control regions in the CON. These
215 increases in FC would have been difficult to observe using the focal recording techniques
216 traditionally employed to study plasticity. Thus, understanding the total impact of disuse on
217 brain function requires consideration of plasticity at multiple spatial scales.
218

The high degree of network specificity seen in disuse-driven plasticity is a powerful demonstration of the validity of individual-specific rs-fMRI network parcellations. It could have been the case that casting produced a complex pattern of FC changes involving many brain systems. Instead, we found that virtually all of the regions showing increased connectivity with the disused motor cortex belonged to a single network, the CON. Thus, large-scale functional networks seem to be a fundamental unit of brain organization, important not only for understanding patterns of activation during cognitive processes, but also for understanding whole-brain patterns of plasticity.

Spontaneous Activity Pulses Alter Functional Connectivity

The network-specific increases in FC between the disused L-SM1$_{ue}$ and the CON likely reflect the emergence of synchronized spontaneous activity pulses in these regions during casting. FC is a measurement of the temporal correlation of spontaneous activity between brain regions. Two complementary analyses (pulse censoring and pulse addition) suggested that pulses contributed to increases in measured FC between disused motor regions and the CON. Many studies have reported increased FC in neuropsychiatric conditions, e.g., Parkinson's disease (33) and Major Depressive Disorder (34). Perhaps some previously reported FC increases could reflect spontaneous activity pulses, similar to those caused by limb disuse. Going forward, spontaneous activity pulses, and the network-specific FC changes they produce, could serve as a biCast3ker of recent disuse and states of heightened plasticity (35).

Decreases in connectivity within the somatomotor system were not fully explained by spontaneous activity pulses. Although the pulse addition analyses showed that spontaneous activity pulses could contribute to decreases in connectivity observed during casting, both the pulse censoring and pulse addition analyses suggested that at least part of the observed

244 decrease in connectivity occurred independently of pulses. Loss of typical co-activation of L-
245 $SM1_{ue}$ and R-$SM1_{ue}$ during daily behavior (31) likely contributed to cast-driven connectivity
246 decreases, consistent with the widely held hypothesis that FC is maintained by a Hebbian-like
247 mechanism that depends on co-activation of brain regions during behavior (19, 36-39).
248

249 **Disuse Impacts Cingulo-opercular Network (CON) Important for Executive Control**

250 The importance of control systems in the human brain has been recognized for several
251 decades (7), but our understanding of these systems has changed dramatically over time and
252 continues to evolve (40). Disentangling the roles of two networks mediating executive control,
253 the cingulo-opercular and frontoparietal networks, has relied largely on complex task designs
254 such as task-switching (21) and slow-reveal paradigms (41). Here, we have demonstrated that
255 a new approach, whole-brain precision functional mapping combined with anatomically specific
256 disuse paradigms, can shed new light on the network interactions that support human
257 cognition and behavior. Although the brain contains several suspected control networks
258 beyond the CON, such as the frontoparietal (FPN), dorsal attention (DAN), ventral attention
259 (VAN) and salience (SAL) networks, disused motor regions showed increased FC only with the
260 CON. The CON is thought to initiate goal-directed behaviors and maintain executive control
261 settings in relation to task objectives (1, 19). The increased FC between disused L-$SM1_{ue}$ and
262 the CON during casting suggests either 1) circuits within the CON were also disused during
263 casting, 2) the CON helps to maintain disused motor circuitry, or 3) spontaneous activity
264 pulses can spread along functional connections to neighboring brain regions in network space.
265

266 Spontaneous activity pulses may have emerged in the CON because its use was also reduced
267 during casting. We previously suggested that spontaneous activity pulses found in motor
268 regions may have been caused by disuse-driven changes in local inhibitory physiology (31,

42). The CON is generally thought to represent task sets, abstract parameters and motor programs governing goal-driven behaviors (1, 19). Task sets can be applied to multiple motor effectors (e.g., right hand, left index finger, etc.), so it would be reasonable to think that casting one extremity would not cause disuse of the CON. However, at least two sets of circuits within the CON may have been disused during casting: circuits that represent bimanual behaviors and circuits that convey task sets to effector-specific downstream regions (e.g., L-SM1$_{ue}$). During casting, many of the task sets previously used to control the dominant upper extremity (e.g., inserting a key into a lock) could have been used to control the non-dominant extremity. However, task sets requiring bimanual coordination (e.g., fastening a belt) could not be applied to an alternative set of motor effectors and may have become disused. Another set of CON circuits that may have been disused are the circuits that convey task set information to effector-specific brain regions. The CON contains both somatotopically organized regions (e.g., SMA, SII) and non-somatotopic regions (e.g., anterior insula). Recent work shows that the SMA and SII, as well as regions of the basal ganglia, may act as hubs that connect the rest of the CON to the somatomotor network (27, 43). Such circuits could potentially undergo disuse during casting of one extremity.

An alternative possibility is that inputs from the CON to L-SM1$_{ue}$ served a homeostatic function during disuse, helping to maintain motor circuits that are typically maintained through active use. We previously suggested that spontaneous activity pulses may help to maintain the organization of disused brain circuits (31). Perhaps pulses are triggered by the CON, which is the system typically responsible for initiating activation of the somatomotor network (1).

Spontaneous activity pulses may also have originated in the disused somatomotor circuits and spread along functional connections to brain regions that were not affected by casting. The

294 CON is immediately adjacent to the somatomotor network in network space (Fig. 2*A*). Previous
295 work in mice found that spontaneous activity bursts in somatosensory cortex, caused by local
296 pharmacogenetic suppression of inhibitory interneurons, spread to other functionally
297 connected regions not targeted by the experimental manipulation (44). An interesting question
298 for future research is whether the CON would show spontaneous activity pulses following
299 disuse of brain systems other than the somatomotor network, such as networks supporting
300 visual and auditory processing, spatial navigation, or social cognition.
301

302 **Two Complementary Mechanisms for Functional Network Plasticity**

303 Extensive whole-brain imaging before, during and after casting revealed that disuse-driven
304 spontaneous activity pulses occur not only in primary motor and somatosensory areas, but
305 also in higher-order brain regions responsible for executive control over behavior. The
306 emergence of spontaneous activity pulses during casting produced increases in FC that were
307 highly focal in network space, specifically occurring between disused motor regions and the
308 CON. Decreases in connectivity between disused motor circuits and the remainder of the
309 somatomotor system, however, were not explained by spontaneous activity pulses. Thus,
310 disuse may drive network plasticity through two complementary mechanisms. Decreased
311 coactivation of brain regions during disuse might drive Hebbian-like disconnection between
312 disused and still-active somatomotor circuits. Spontaneous activity pulses, which contributed to
313 increased connectivity with the CON, may help preserve disused circuits for future
314 reintegration and use. Together, these two network plasticity mechanisms—Hebbian-like and
315 pulse-mediated—may represent a network-focal “stand-by mode” that allows the brain to
316 isolate disused circuits while simultaneously protecting them from premature functional
317 degradation.

Acknowledgements:
We thank Kristen M. Scheidter and Annie L. Nguyen for help in collecting MRI data and Ryan V. Raut for his comments on the manuscript. This work was supported by NIH grants NS110332 (D.J.N.), NS088590 (N.U.F.D.), TR000448 (N.U.F.D.), MH96773 (N.U.F.D.), MH122066 (N.U.F.D.), MH1000872 (T.O.L.), MH112473 (T.O.L.), NS090978 (B.P.K.), MH104592 (D.J.G.), NS080675 (M.E.R.), NS098577 (to the Neuroimaging Informatics and Analysis Center); the US Department of Veterans Affairs Clinical Sciences Research and Development Service grant 1IK2CX001680 (E.M.G.); Kiwanis Neuroscience Research Foundation (N.U.F.D.); the Jacobs Foundation grant 2016121703 (N.U.F.D.); the Child Neurology Foundation (N.U.F.D.); the McDonnell Center for Systems Neuroscience (D.J.N., T.O.L., A.Z., B.L.S., and N.U.F.D.); the McDonnell Foundation (S.E.P.), the Mallinckrodt Institute of Radiology grant 14-011 (N.U.F.D.); the Hope Center for Neurological Disorders (N.U.F.D., B.L.S., and S.E.P.).

Author Contributions:
D.J.N., T.O.L., C.R.H., A.Z.S., and N.U.F.D. designed the study. D.J.N., C.R.H., J.M.H., M.O., and N.U.F.D. collected the data. D.J.N. and E.M.G. analyzed the data. D.J.N., E.M.G., T.O.L., N.A.S., D.F.M., S.J.G., A.Z., A.N.N., B.A., A.R.C., B.P.K., D.J.G., M.E.R., S.E.P., A.Z.S., and N.U.F.D. interpreted the results. D.J.N. and N.U.F.D. wrote the manuscript with input from all other authors.

Declaration of interests:
The authors declare the following competing financial interest: N.U.F.D. is co-founder of NOUS Imaging.

METHODS

318 ***Human Participants***

319 Participants were three healthy, adult volunteers. Details are described in Newbold *et al.* (31).

320 ***Experimental Intervention***

321 We constrained the dominant upper extremity for two weeks by fitting each participant with a fiberglass
322 cast. Casts extended from just below the shoulder to past the fingertips. Details are described in
323 Newbold *et al.* (31).

324 ***MRI Acquisition***

325 Participants were scanned every day of the experiment for 42-64 consecutive days. We collected 30
326 minutes of resting-state functional MRI (rs-fMRI) data every day of the experiment, as well as also task
327 fMRI and T1- and T2-weighted structural scans. Acquisition parameters and procedures are detailed in
328 Newbold *et al.* (31).

329 ***MR Image Processing***

330 Preprocessing of structural and functional images, denoising of resting-state fMRI data, and cortical
331 surface projection were performed previously (31). Fully processed data are available in the Derivatives
332 folder of the Cast-Induced Plasticity dataset on OpenNeuro (www.openneuro.org/datasets/ds002766).

333 ***ROI Selection***

334 The region of the left primary somatomotor cortex controlling the casted upper extremity (L-SM1$_{ue}$) was
335 located individually in each participant using task fMRI. Details of the task analysis and region of
336 interest (ROI) selection are described in Newbold *et al.* (31). The L-SM1$_{ue}$ ROI was used here to
337 generate seed maps (Fig. 1, S1), to analyze spatial specificity of whole-brain functional connectivity
338 changes (Fig. 3*B*, S3) and to measure FC between L-SM1$_{ue}$ and the dorsal anterior cingulate cortex
339 (dACC) for the removable cast control experiment (Fig. S4), the pulse censoring analysis (Fig. 4) and
340 the pulse addition analysis (Fig. 5, S7).

Individual-specific sets of parcels spanning the entire cerebral cortex were previously generated for each participant using a functional connectivity gradient-based approach, and each parcel was assigned to one of 17 canonical functional networks using a graph theory-based community detection algorithm (22, 31). Cortical parcels were used here to display functional connectivity changes in anatomical (Fig. 1-2, 5, S1-S2, S4-S6) and network space (Fig. 2, S2). We also generated a set of subcortical and cerebellar parcels by assigning each voxel to the functional network with which it showed the strongest functional connectivity and then grouping adjacent voxels with matching network assignments into parcels. Sets of cortical, subcortical and cerebellar parcels were used to examine changes in FC between all pairs of brain regions (Fig. 3, S2).

A subset of parcels corresponding to the left primary somatomotor cortex (L-$SM1_{ue}$) was previously generated by selecting all left-hemisphere parcels assigned to the upper-extremity somatomotor network, excluding any parcels that fell outside of the pre- and post-central gyri (31). Functional connections between L-$SM1_{ue}$ parcels and all other parcels were averaged to generate parcel-wise seed maps (Fig. 1-2, 5, S1-S2, S4-S6) and to quantify the spatial specificity of FC changes between all cortical, subcortical and cerebellar parcels (Fig. 3, S3).

Individual-specific ROIs in the left dorsal anterior cingulate cortex (L-dACC) were selected using pulse analysis of variance (ANOVA) maps, which were previously generated for each participant (31). ROIs were selected within a large anatomical region, automatically labeled by FreeSurfer (union of caudal anterior cingulate gyrus, posterior cingulate gyrus, and superior frontal gyrus). We first located the vertex showing the maximum ANOVA F-statistic and then iteratively expanded the ROI by selecting neighboring vertices in descending order of F-statistic, until the ROI included 100 vertices. The L-dACC ROI was used to measure FC between L-$SM1_{ue}$ and the L-dACC for pulse censoring (Fig. 4) and pulse addition analyses (Fig. 5, S7).

364 ***Functional Connectivity Measurement***

365 Mean rs-fMRI time series were extracted from the L-SM1$_{ue}$ ROI and each cortical, subcortical and
366 cerebellar parcel by averaging the time series of all vertices/voxels within the ROI/parcel. Vertex-wise
367 functional connectivity (FC) seed maps were generated for each session by computing a Pearson
368 correlation between the mean rs-fMRI time series from the L-SM1$_{ue}$ ROI and the time series from every
369 vertex. Frames with high head motion, identified previously (31), were excluded from FC calculations.
370 Vertex-wise seed maps were averaged across sessions before, during and after casting (Pre, Cast,
371 Post; Fig. 1, S1).

372 FC between all pairs of cortical, subcortical and cerebellar parcels was measured as pairwise
373 correlations of all mean rs-fMRI time series, excluding high-motion frames, producing a correlation
374 matrix for each session. Correlation matrices were averaged over Pre, Cast and Post period. FC
375 changes during casting and recovery were computed as the differences between correlation matrices
376 (casting = Cast – Pre; recovery = Post – Cast). Full Cast – Pre differences matrices are shown in
377 Figure S3. Parcel-wise difference seed maps showing changes in L-SM1$_{ue}$ FC during casting and
378 recovery (Fig. 1-2, S1-S2) were computed by averaging together columns of the difference matrices
379 corresponding to the L-SM1$_{ue}$ parcels (see *ROI selection,* above).

380 ***Spring Embedding***

381 Cortical parcels were displayed in network space using force-directed ("spring-embedded") graphs(45),
382 generated with Gephi (https://gephi.org/). Graph weights were taken from parcel-wise correlation
383 matrices averaged across all sessions prior to casting (Pre). Graphs were thresholded to include only
384 the top 0.2% of pairwise functional connections. We initially examined graphs using an edge threshold
385 of 0.1%, but several parcels with large FC changes were disconnected from the main graph. Thus, we
386 selected the 0.2% connection threshold to display all key findings (Fig. 2, S2).

Functional Connectivity Changes by Network

To test which functional networks showed large changes in FC with L-SM1$_{ue}$ during casting, parcel-wise L-SM1$_{ue}$ seed maps were compared to individual-specific network maps. Parcel-wise L-SM1$_{ue}$ difference seed maps (Cast – Pre) were thresholded to contain the top 5% of parcels showing FC increases/decreases. FC increases (Cast > Pre) and decreases (Cast < Pre) were examined separately. The number of supra-threshold parcels in each cortical network is shown in Figure 2. Alternative thresholds (top 1%, 10% and 20%) all yielded similar results. Networks containing a greater number of FC increases/decreases than expected by chance were identified by comparing the number of supra-threshold parcels found using each participant's true network map to the number of parcels found using spatially permuted network maps (see *Statistical analyses*, below).

Whole-brain Analyses of Functional Connectivity Changes

The spatial specificity of whole-brain plasticity was examined by comparing changes in FC between all cortical, subcortical and cerebellar parcels to individual-specific functional network maps. We examined the top 50 changes in FC (25 greatest increases and 25 greatest decreases). A change in FC between two parcels was counted as involving L-SM1$_{ue}$ if either of the two parcels was an L-SM1$_{ue}$ parcel. The number L-SM1$_{ue}$ changes found using each participant's true network map was compared to the number of L-SM1$_{ue}$ changes found using spatially permuted network maps (see *Statistical analyses*, below).

To examine whole-brain FC changes at a finer spatial resolution, we examined differences in FC between all cortical, subcortical and cerebellar vertices/voxels. We computed the magnitude of whole-brain FC change between each vertex/voxel as the sum of squared FC changes between that vertex/voxel and every other gray-matter vertex/voxel (Fig. 3, S3). We tested if whole-brain FC change was higher in L-SM1$_{ue}$ than in the rest of the brain by comparing the mean magnitude of whole-brain FC change inside of each participant's true L-SM1$_{ue}$ ROI to the mean magnitude of whole-brain FC change inside of spatially rotated ROIs (see *Statistical analyses*, below).

412 ***Spatial and Temporal Comparisons of Pulses and FC Changes***

413 To generate a parcel-wise map of spontaneous activity pulses, we extracted rs-fMRI time series from
414 every cortical, subcortical and cerebellar parcel surrounding each detected pulse (13.2 seconds before
415 to 17.6 seconds after each pulse peak). Pulse peaks were detected previously (31). We then performed
416 an ANOVA on the extracted time series (Fig. S5*B*). The spatial distribution of ANOVA F-statistics was
417 compared to the spatial distribution of L-SM1$_{ue}$ FC changes using a Pearson correlation across parcels.

418 We also compared the number of pulses detected during each rs-fMRI scan (31) to the FC measured
419 between L-SM1$_{ue}$ and L-dACC (Fig. S4*C*), using a Pearson correlation.

420 ***Pulse Censoring Analyses***

421 To assess the contribution of large, detectable spontaneous activity pulses (>0.4% rs-fMRI signal
422 change) to FC changes observed during casting, frames surrounding each pulse (13.2 seconds before
423 to 17.6 seconds after each pulse peak) were excluded from FC calculations. Pulse detection criteria
424 were identical to those used previously (31). We plotted FC measured between L-SM1$_{ue}$ and L-dACC
425 during each session before casting (Pre), during casting (Cast) and during casting with pulses excluded
426 (Cens; Fig. 4*B*). We compared Cast vs. Pre FC measurements and Cens vs. Cast FC measurements
427 using t-tests (see *Statistical analyses*, below). We also generated difference seed maps showing FC
428 changes between L-SM1$_{ue}$ and all cortical parcels due to censoring (Cens – Cast; Fig. 4*C*, S6).

429 ***Pulse Addition Analyses***

430 To assess the contribution to FC changes of pulses with a hypothetical full magnitude distribution,
431 including pulses that were too small (<0.4% rs-fMRI signal change) to distinguish from ongoing
432 spontaneous activity fluctuations, we created simulated rs-fMRI time series containing a full distribution
433 of pulses. We first generated a histogram showing the magnitude distribution of detected pulses.
434 Magnitudes were grouped into bins with a width of 0.5%-signal-change. We then fit a log-normal
435 distribution to the observed pulse magnitudes using a least-squares approach (Fig. 5*A*). This provided
436 an estimate of the full pulse magnitude distribution, including pulses that were too small to detect. We

437 then added the mean pulse time series to the baseline (Pre) rs-fMRI time series, drawing pulse
438 magnitudes from the full log-normal distribution (example shown in Fig. 5*B*). The number of pulses
439 added was selected so that the number of large pulses (>0.4% signal change) would match the number
440 of pulses detected in each participant in an average Cast scan. We then computed FC of the baseline
441 time series (Pre) and the time series with added pulses (Sim; Fig. 5*C*). Finally, we applied the same
442 pulse censoring strategy described above to the simulated time series and computed FC after
443 censoring (Cens; Fig. 5*C*). Because pulse magnitudes were drawn from a full log-normal distribution,
444 only a portion of the added pulses were detected and censored. We compared Sim vs. Pre FC
445 measurements and Cens vs. Sim FC measurements using t-tests (see *Statistical analyses*, below). The
446 simulation and censoring procedures were repeated using triangular and exponential magnitude
447 distributions (Fig. S7). We also generated difference seed maps showing FC changes between L-
448 $SM1_{ue}$ and all cortical parcels due to pulse simulation (Sim – Pre; Fig. 5*D*, S8).

449 ***Statistical Analyses***

450 All statistical tests were performed identically for each participant. Whenever appropriate, we used
451 simple parametric statistical tests:

452 - Spatial similarity between anatomical maps was tested using a Pearson correlation across
453 parcels (Cast1: d.f. = 566; Cast2: 578; Cast3: 624). Spatial correlations were computed
454 between the following maps:
455 - FC changes during casting (Cast – Pre) vs. FC changes during recovery (Post – Cast;
456 Fig. 1*B*)
457 - FC changes during casting (Cast – Pre) vs. pulse ANOVA (F-statistic; Fig. S5)
458 - FC changes during casting (Cast – Pre) vs. FC changes due to pulse censoring (Cens –
459 Cast; Fig. 4*C*, S6)
460 - FC changes due to pulse censoring (Cens – Cast) vs. residual FC changes after pulse
461 censoring (Cens – Pre; Fig. S6)

462 ○ FC changes during casting (Cast – Pre) vs. FC changes due to simulated pulses (Sim –
463 Pre; Fig. 5*D*, S8)

464 • The number of pulses detected during each scan was compared to the FC measured between
465 L-SM1$_{ue}$ and L-dACC using a Pearson correlation (Cast1: d.f. = 45; Cast2: 61; Cast3: 40; Fig.
466 S5*C*).

467 • FC between L-SM1$_{ue}$ and L-dACC measured during each session of the cast period (Cast1: n =
468 13 sessions; Cast2: 13; Cast3: 14) was compared to FC during each session of the pre period
469 (Cast1: n = 10; Cast2: 12; Cast3: 14) using a two-sided, unpaired t-test (Cast1: d.f. = 21, Cast2:
470 23, Cast3: 26; Fig. S5*B*).

471 • FC between L-SM1$_{ue}$ and L-dACC measured using the full time series (motion-censored only) of
472 each session of the cast period (Cast1: n = 13 sessions; Cast2: 13; Cast3: 14) was compared to
473 FC measurements of the same sessions excluding pulses (motion- and pulse-censored) using a
474 one-sided, paired t-test (Cast1: d.f. = 24, Cast2: 24, Cast3: 26; Fig. 4*B*).

475 • FC between L-SM1$_{ue}$ and L-dACC measured during each session of the pre period (Pre; Cast1:
476 n = 10; Cast2: 12; Cast3: 14) was compared to FC measurements of the same sessions after
477 adding simulated pulses (Sim) using a two-sided, paired t-test (Cast1: d.f. = 18, Cast2: 22,
478 Cast3: 26; Fig. 5*C*).

479 • FC between L-SM1$_{ue}$ and L-dACC measured using the full time simulated series (Sim; motion-
480 censored only; Cast1: n = 10; Cast2: 12; Cast3: 14) was compared to FC measurements of the
481 same sessions excluding pulses (motion- and pulse-censored) using a two-sided, paired t-test
482 (Cast1: d.f. = 18, Cast2: 22, Cast3: 26; Fig. 5*C*).

483 When parametric statistical tests were not appropriate to test a specific hypothesis, we tested results
484 against a null distribution generated via permutation resampling. In each case, our null hypothesis was
485 that observed effects had no spatial relationship to ROIs/functional networks and any overlap occurred
486 by chance. For vertex-wise ROIs, we modeled the null hypothesis by rotating the ROI around the
487 cortical surface 1,000 times (46, 47). For functional networks, we modeled the null hypothesis by

488 permuting the network assignments of parcels 1,000 times. Each permuted ROI/network map was used
489 exactly as the actual map in order to compute a null distribution for the value of interest. The P-value
490 reported for each test represents the two-sided probability that a value in the null distribution has a
491 greater magnitude than the observed value. Permutation resampling was used to generate null
492 distributions for the following values:

493 - Overlap of each functional network with increases in L-SM1$_{ue}$ FC during casting (Cast > Pre;
494 number of parcels in top 5%; Fig. 2*B*)
495 - Overlap of each functional network with decreases in L-SM1$_{ue}$ FC during casting (Cast > Pre;
496 number of parcels in top 5%; Fig. 2*C*)
497 - Overlap of L-SM1$_{ue}$ parcels with the 50 largest changes in FC between all pairs of cortical,
498 subcortical and cerebellar parcels (Fig. 3*A*, Fig. S3)
499 - Magnitude of whole-brain FC change in the L-SM1$_{ue}$ ROI (Fig. 3*B*, S3)

500 Since we tested the overlap of L-SM1$_{ue}$ FC increases/decreases with 17 different functional networks, a
501 Benjamini-Hochberg procedure was applied to correct for multiple comparisons, maintaining false
502 discovery rates < 0.05. Each of the three participants constituted a separate replication of the
503 experiment, rather than multiple comparisons, so no correction was necessary for tests repeated in
504 each participant.

505 ***Data Visualization***

506 Regions of interest and whole-brain pulse maps were shown on cortical surfaces generated by
507 FreeSurfer (48) and Human Connectome Project (HCP) Workbench software packages (49). These
508 images were rendered using HCP Workbench (49). Figures showing the greatest differences in
509 functional connectivity across the entire brain in inflated anatomical space (Fig. 3, S3) were rendered
510 using Blender, a free and open-source 3D modeling software package (www.blender.org). To make the
511 large number of changed connections included in these images visually compact, connections following

similar spatial trajectories were drawn toward each other using a previously published mean-shift edge bundling algorithm (50). All other figures were produced using Matlab (www.mathworks.com).

Data Availability

This study used our previously published dataset (31), available on the OpenNeuro database (www.openneuro.org/datasets/ds002766).

Code Availability

All code needed to reproduce our analyses is available on Gitlab (https://gitlab.com/DosenbachGreene/cast-whole-brain).

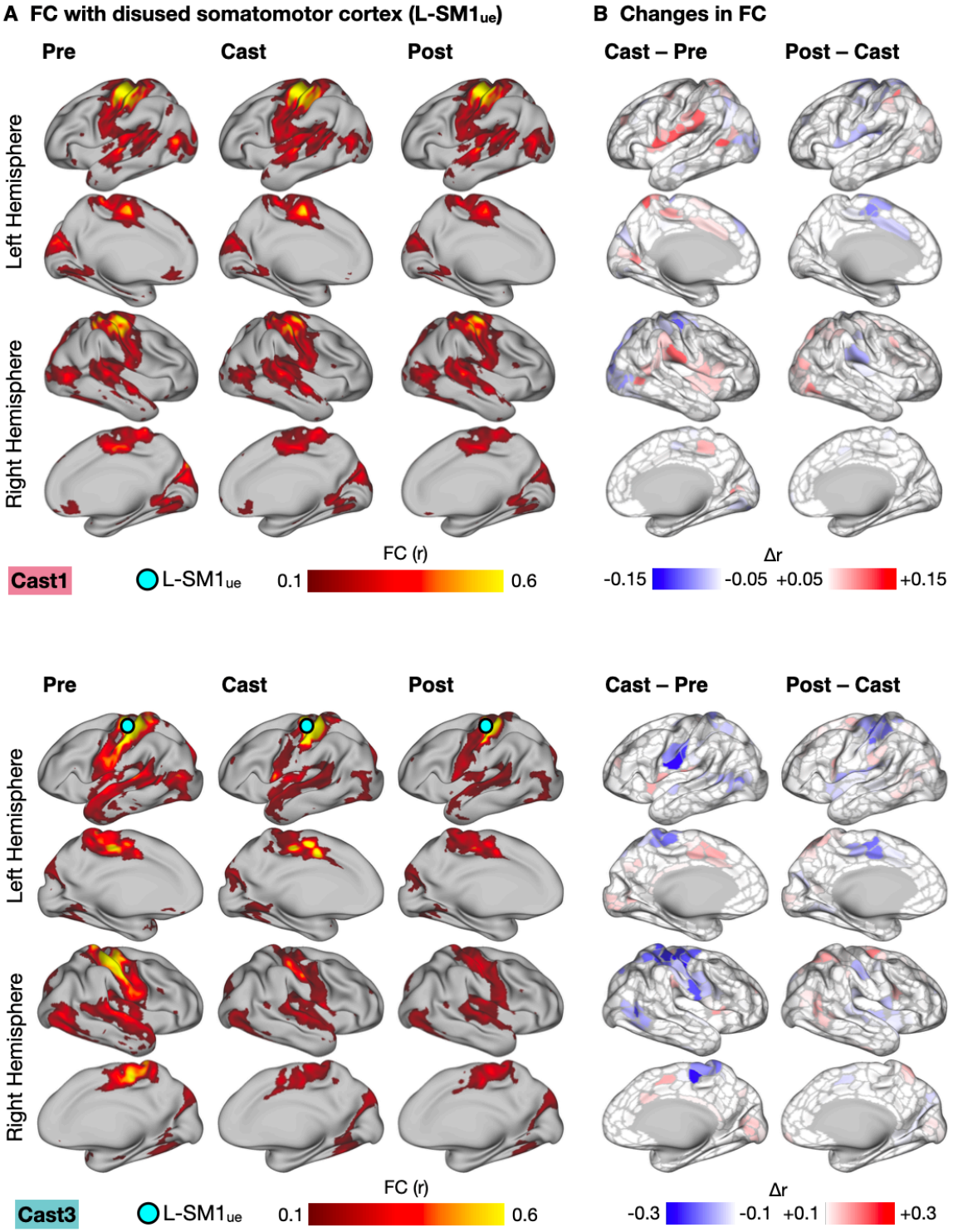

Fig. S1. Functional Connectivity (FC) Changes Involving the Disused Somatomotor Cortex (L-SM1$_{ue}$) in Anatomical Space (All Participants). (A) Seed maps showing FC between L-SM1$_{ue}$ and the remainder of the cerebral cortex in Cast1 (top) and Cast3 (bottom). Seed maps were averaged across sessions before, during and after casting (Pre, Cast, Post). (B) Subtraction maps showing changes in FC during casting (Cast – Pre) and recovery (Post – Cast). Differences are shown on sets of 506 (Cast1) and 626 (Cast3) individual-specific cortical parcels. For Cast1 and Cast2, these parcels were previously generated and published (Gordon, 2017). We applied identical methods to generate a set of parcels for Cast3.

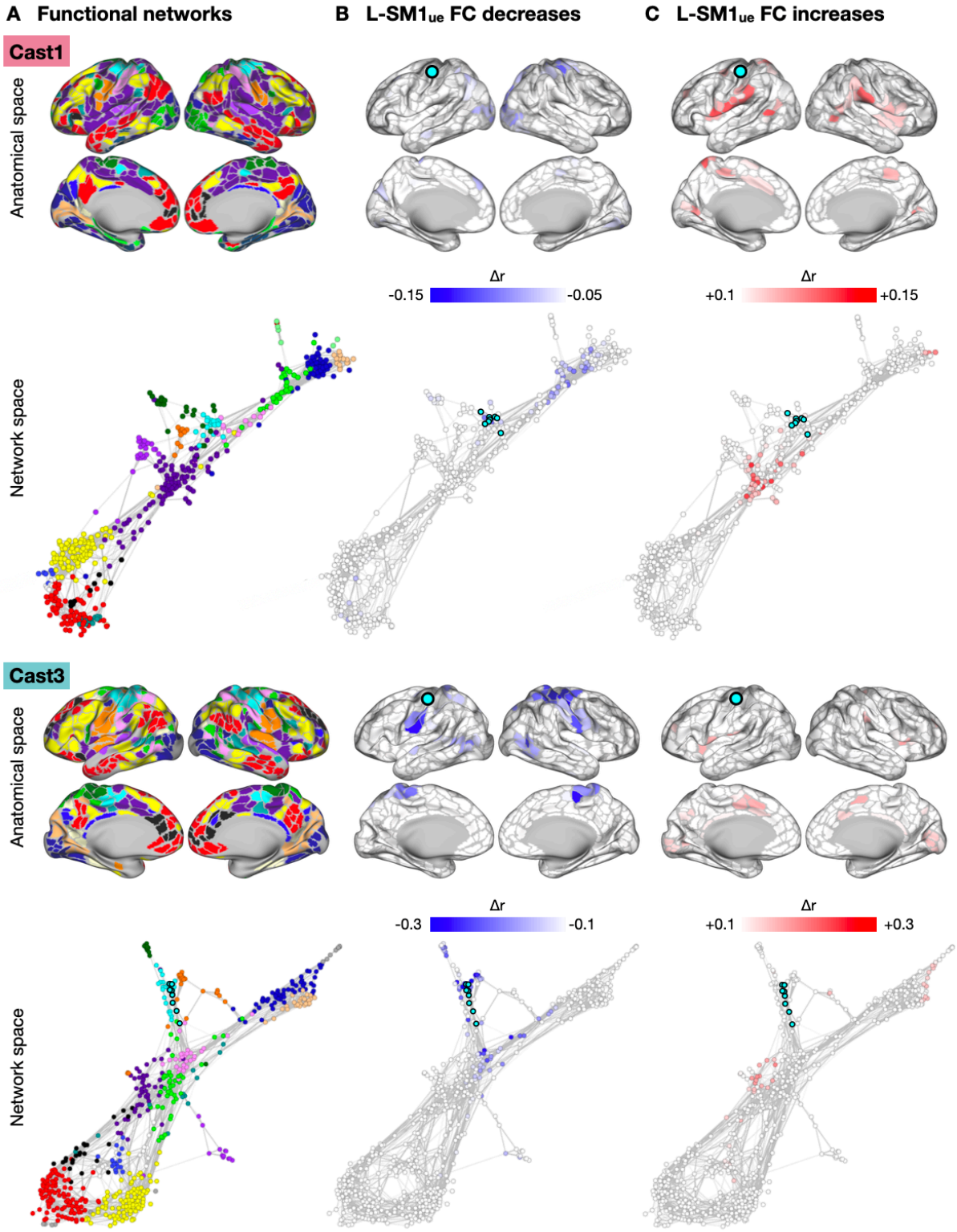

Fig. S2. Functional Connectivity (FC) Changes Involving the Disused Somatomotor Cortex (L-SM1$_{ue}$) in Anatomical and Network Space in Cast1 and Cast3. (A) Maps of 17 canonical functional networks in Cast1 (top) and Cast3 (bottom). Networks are shown in anatomical space (inflated cortical surfaces) and network space (spring-embedded graphs based on Pre scans). See Figure 2 for network color key. (B) Subtraction maps showing disuse-driven decreases in functional connectivity (FC) with left somatomotor cortex (L-SM1$_{ue}$) in anatomical space and network space. (C) Subtraction maps showing disuse-driven increases in FC with L-SM1$_{ue}$ in anatomical and network space.

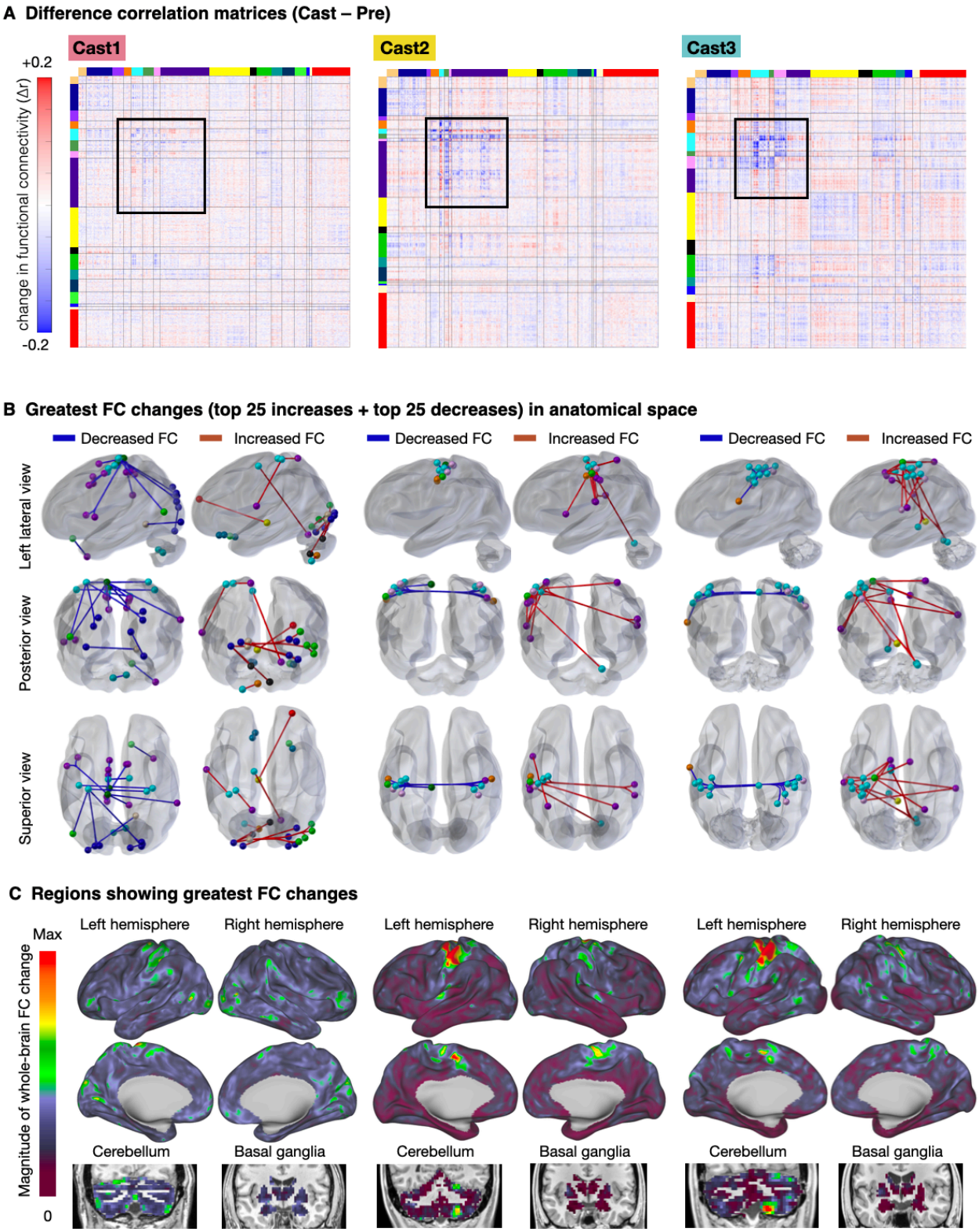

Fig. S3. Whole-brain Patterns of Disuse-driven Plasticity. (A) Matrices showing changes in functional connectivity (FC) between all pairs of individual specific cortical, subcortical and cerebellar parcels during casting (Cast1: 744 parcels, Cast2: 733; Cast3: 761**).** (B) 50 largest changes in FC shown in anatomical space. (C) Magnitude of whole-brain FC change, computed as the sum of squared FC changes between each vertex/voxel and every other gray-matter vertex/voxel.

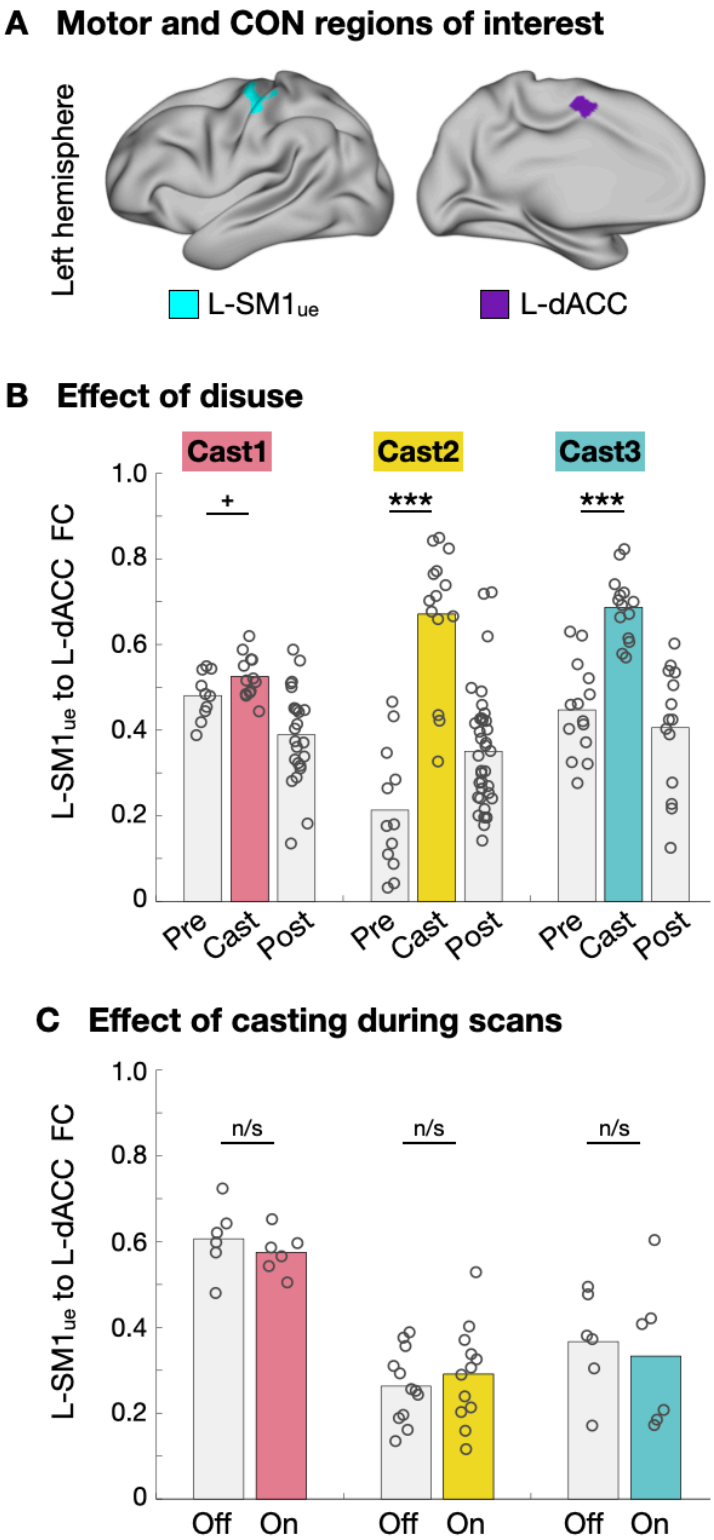

Fig. S4. Connectivity between Disused Somatomotor Cortex and Cingulo-opercular Network during Disuse and Temporary Casting. (A) Example regions of interest (ROIs) in the left primary somatomotor cortex (L-SM1$_{ue}$) and the left dorsal anterior cingulate cortex (L-dACC). (B) Functional connectivity (FC) measured between L-SM1$_{ue}$ and L-dACC before (Pre), during (Cast) and after casting (Post). Two participants (Cast2 and Cast3) show a significant increase in FC during the cast period $^{+}P < 0.1$, $^{*}P < 0.05$, $^{***}P < 0.001$. (C) FC measured between L-SM1$_{ue}$ and L-dACC during both conditions of the control experiment: without casting (Off) and with temporary casts during scans (On). No changes in FC were observed.

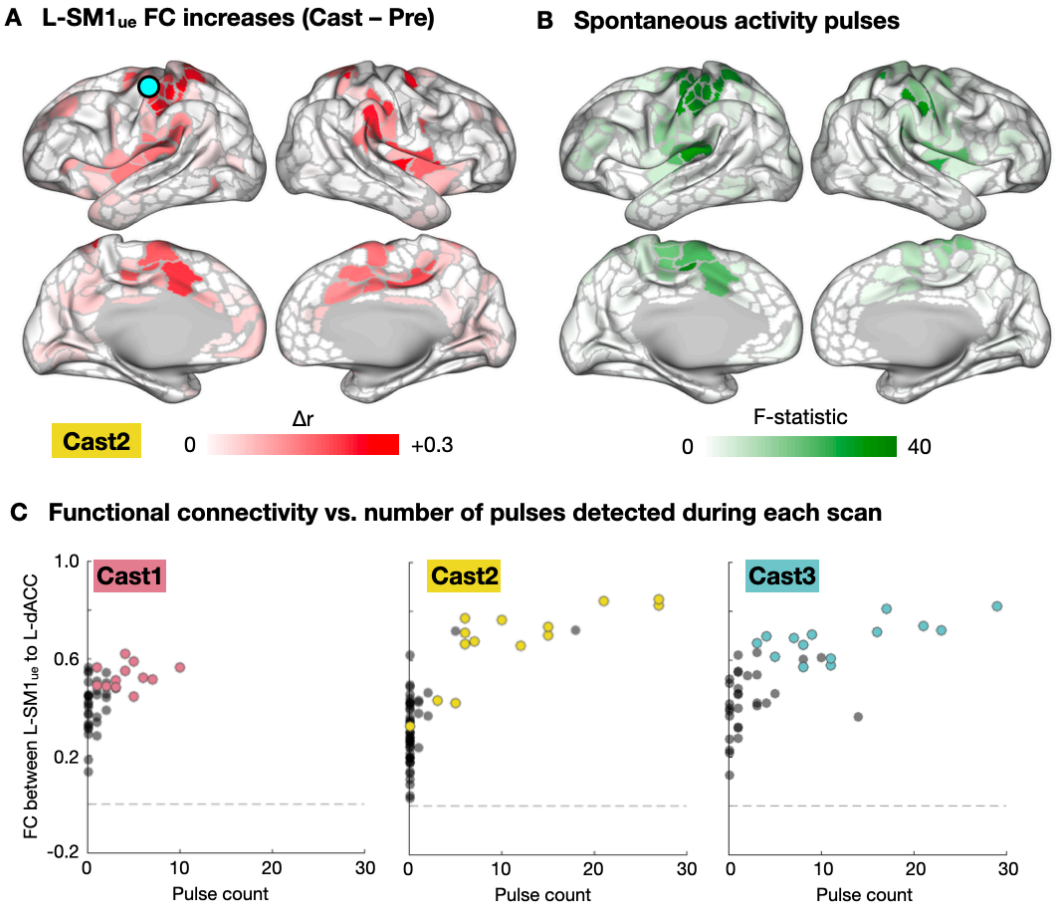

Fig. S5. Relationship of Spontaneous Activity Pulses to Functional Connectivity (FC) Changes. (A) Increases in FC with the disused somatomotor cortex (L-SM1$_{ue}$) during casting, repeated from Figure 2B for reference. (B) Analysis of variance (ANOVA) showing regions with spontaneous activity pulses. ANOVA F-statistic was correlated with FC change in each parcel (Cast1: $r = 0.16$, $P < 0.001$; Cast2: $r = 0.29$, $P < 0.001$; Cast3: $r = 0.06$, $P = 0.12$). (C) Relationship of FC between L-SM1$_{ue}$ and the dorsal anterior cingulate cortex (dACC; cingulo-opercular network (CON)) vs. the number of pulses detected. Each dot represents one 30-minute scan. Colored dots represent scans during the cast period. For all participants, FC between L-SM1$_{ue}$ and dACC was significantly correlated with the number of pulses detected (Cast1: $r=0.74$, $P<0.001$; Cast2: $r=0.57$, $P<0.001$; Cast3: $r=0.73$, $P<0.001$).

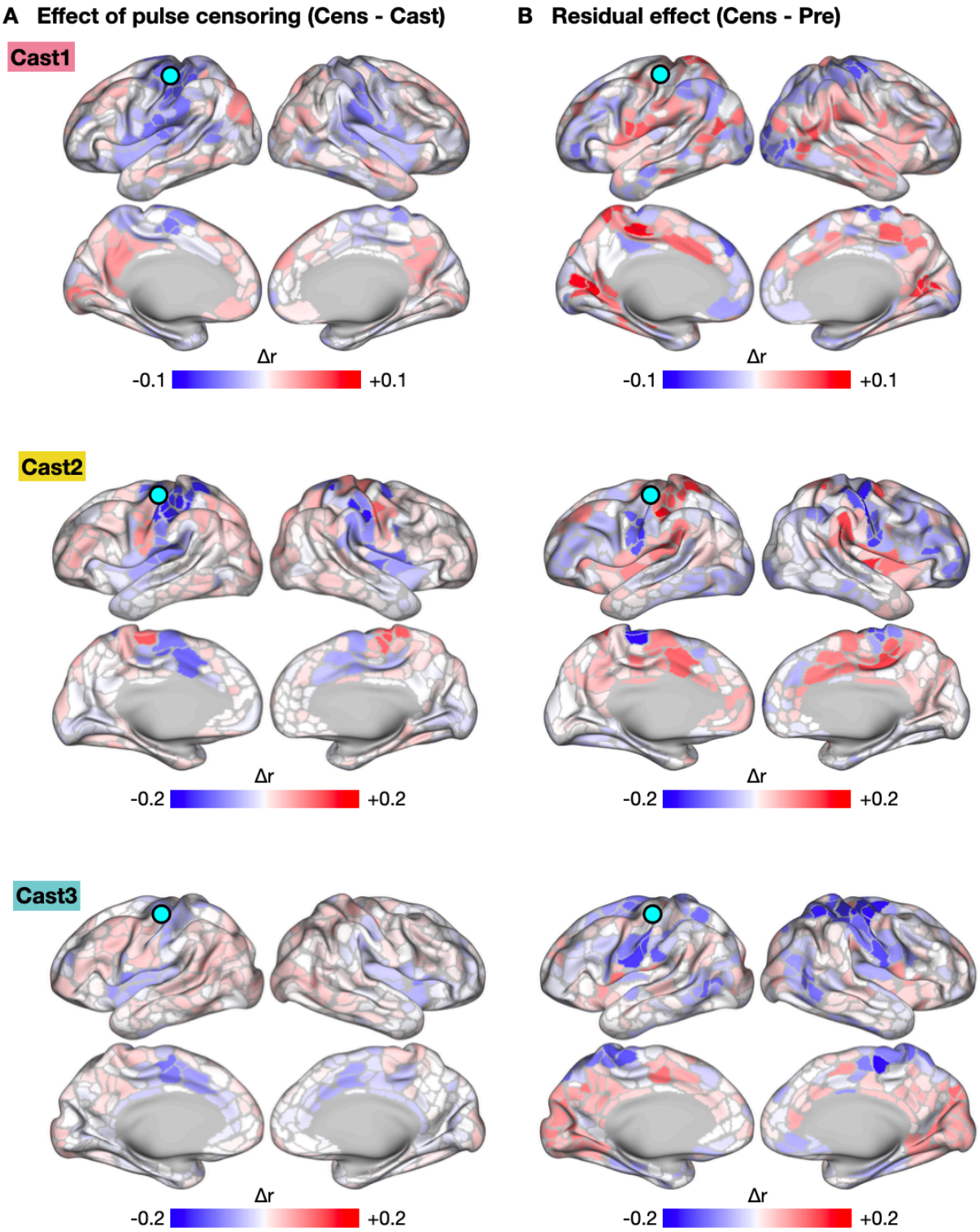

Fig. S6. Functional Connectivity (FC) Changes Explained by Spontaneous Activity Pulses. (A) Subtraction map showing changes in L-SM1$_{ue}$ FC due to pulse censoring. The spatial pattern of FC changes due to pulse censoring was negatively correlated with FC changes during casting (Cast1: r = -0.35, P < 0.001; Cast2: r = -0.90, P < 0.001; Cast3: r = -33, P < 0.001). (B) Subtraction map showing residual FC changes during casting after pulse censoring. The spatial pattern of residual FC changes was negatively correlated with the effect of pulse censoring (Cast1: spatial correlation, r = -0.23, P < 0.001; Cast2: r = -0.76, P < 0.001; Cast3: r = -0.18; P < 0.001).

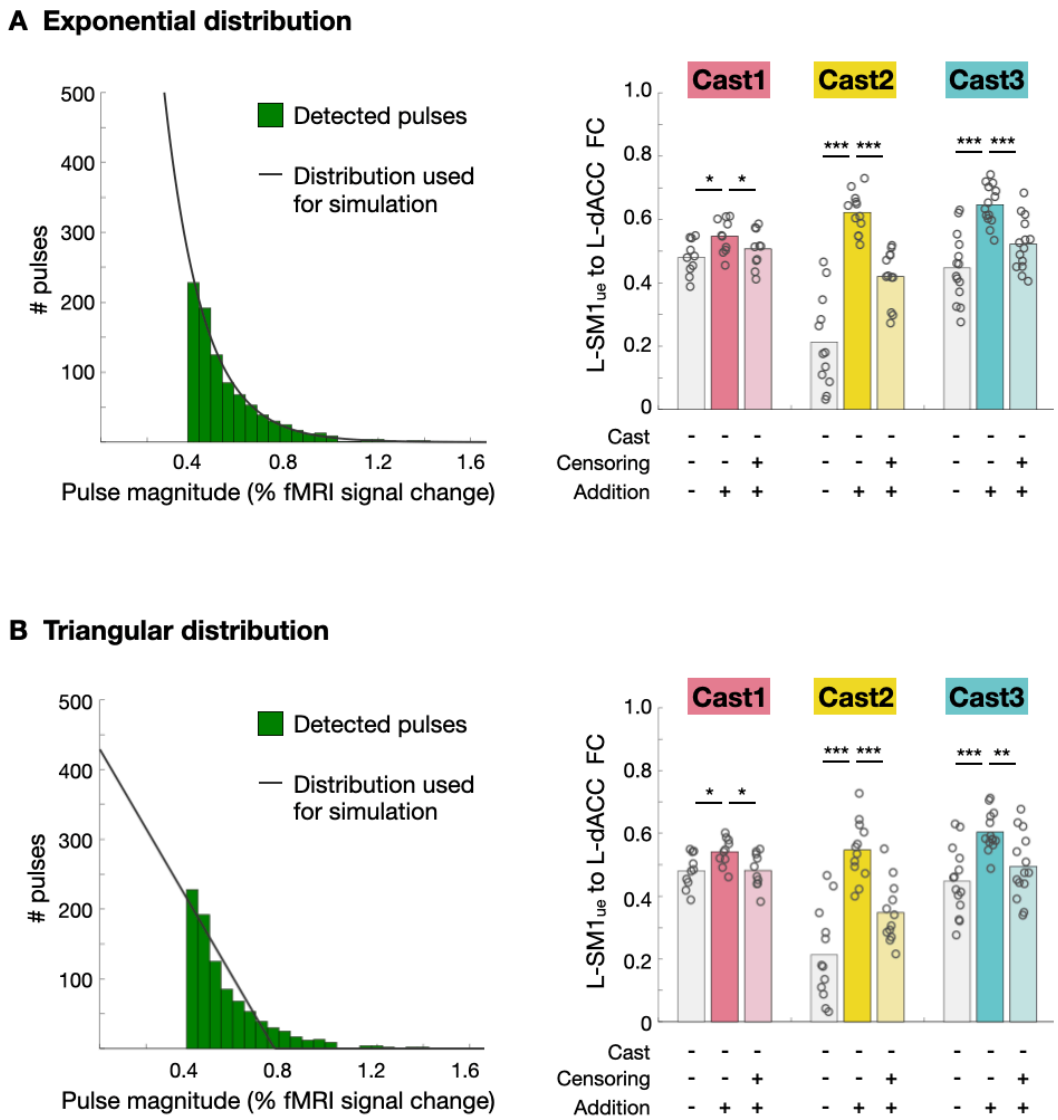

Fig. S7. Alternative Distributions for Pulse Magnitudes. (A) Exponential distribution. *Left:* Histogram of pulse magnitudes (peak fMRI signal), pooled across all participants. An exponential distribution (black line) was fit to the data using a least-squares approach. *Right:* Adding simulated pulses, with magnitudes drawn from the exponential distribution, increased FC between L-SM1$_{ue}$ and L-dACC. Censoring simulated pulses partially reduced FC increases. *P<0.05, ***P<0.001. (B) Triangular distribution. *Left:* Histogram of pulse magnitudes (peak fMRI signal), pooled across all participants. A linear distribution (black line) was fit to the data using a least-squares approach. *Right:* Adding simulated pulses, with magnitudes drawn from the linear distribution, increased FC between L-SM1$_{ue}$ and L-dACC. Censoring simulated pulses partially reduced FC increases. *P<0.05, **P<0.01, ***P<0.001.

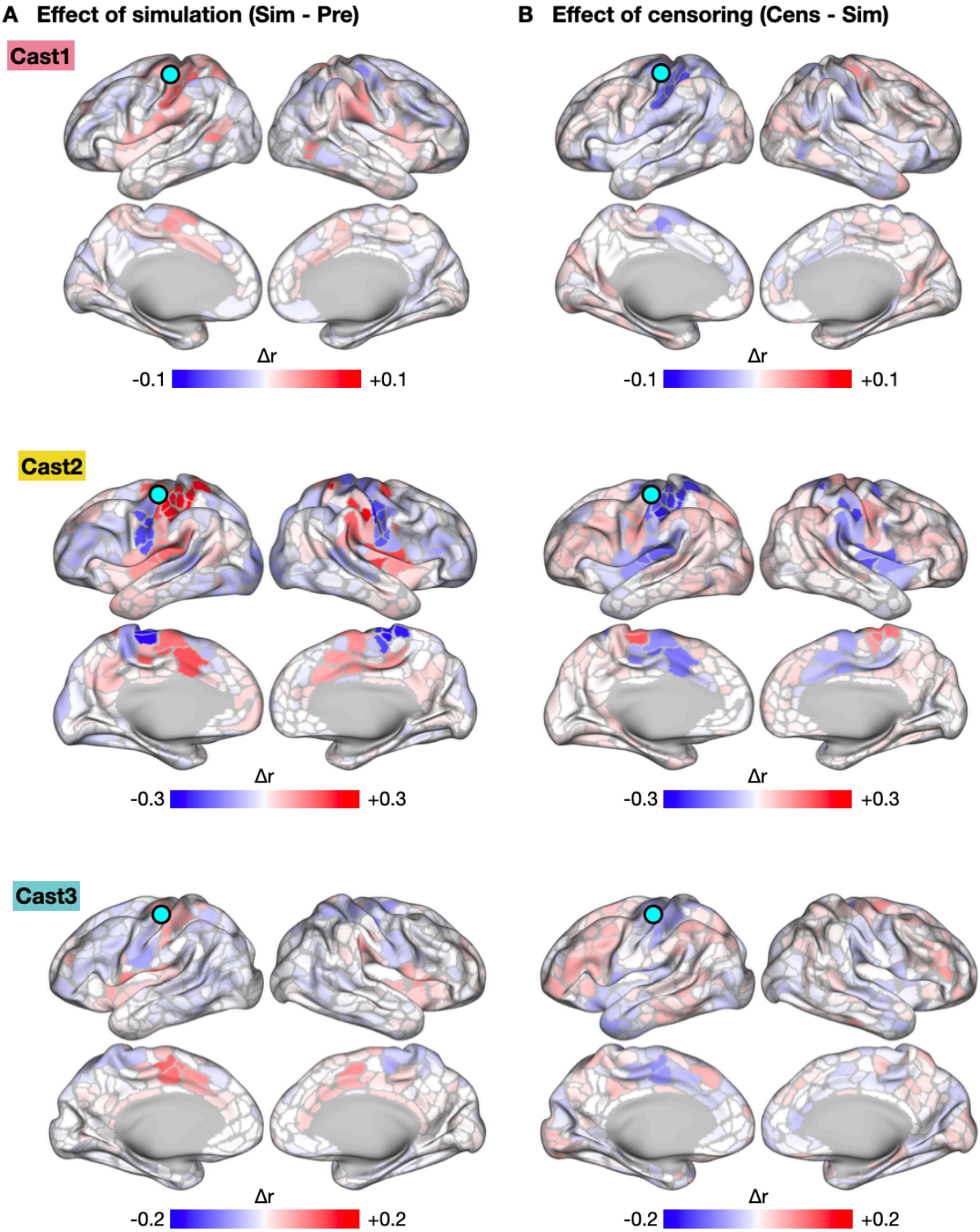

Fig. S8. Functional Connectivity (FC) Changes Caused by Simulated Spontaneous Activity Pulses (All Participants). (A) Subtraction map showing changes in L-SM1$_{ue}$ FC due to addition of simulated pulses. FC changes due to pulse addition closely matched FC changes during casting (Cast1: spatial correlation, $r = 0.44$, $P < 0.001$; Cast2: $r = 0.95$, $P < 0.001$; Cast3: $r = 0.64$, $P < 0.001$). (B) Subtraction map showing effect of censoring simulated pulses. Effects of censoring closely complemented the effect of pulse addition (Cast1: $r = -0.71$, $P < 0.001$; Cast2: $r = -0.96$, $P < 0.001$; Cast3: $r = -0.69$; $P < 0.001$).

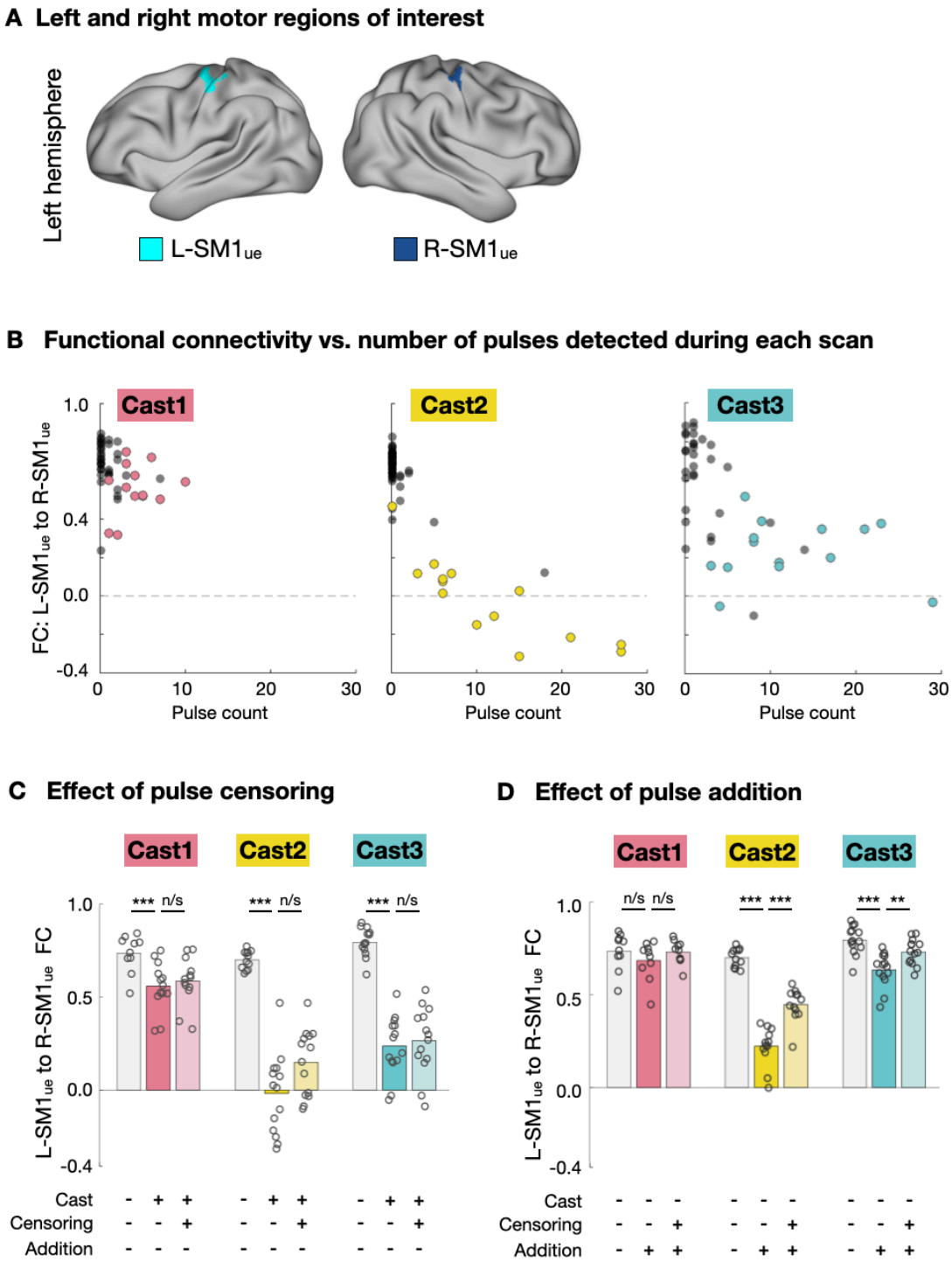

Fig. S9. Functional Connectivity (FC) Decreases Were Not Explained by Spontaneous Activity Pulses. (A) Example regions of interest (ROIs) in the left and right primary somatomotor cortex (L-SM1$_{ue}$ and R-SM1$_{ue}$). (B) Relationship of FC between L-SM1$_{ue}$ and R-SM1$_{ue}$ vs. the number of pulses detected. Each dot represents one 30-minute scan. Colored dots represent scans during the cast period. For all participants, FC between L-SM1$_{ue}$ and R-SM1$_{ue}$ was significantly correlated with the number of pulses detected (Cast1: r=0.74, P<0.001; Cast2: r=0.57, P<0.001; Cast3: r=0.73, P<0.001). (C) Censoring pulses did not reduce the difference between Pre and Cast scans. ***P < 0.001. (D) Adding simulated pulses decreased FC between L-SM1$_{ue}$ and R-SM1$_{ue}$ in two participants (Cast2 and Cast3), but these decreases were much smaller than those observed during casting. ***P < 0.001. **P < 0.01.

REFERENCES

1. N. U. Dosenbach *et al.*, Distinct brain networks for adaptive and stable task control in humans. *Proc Natl Acad Sci U S A* **104**, 11073-11078 (2007).

2. T. N. Wiesel, D. H. Hubel, Comparison of the effects of unilateral and bilateral eye closure on cortical unit responses in kittens. *J Neurophysiol* **28**, 1029-1040 (1965).

3. M. M. Merzenich *et al.*, Topographic reorganization of somatosensory cortical areas 3b and 1 in adult monkeys following restricted deafferentation. *Neuroscience* **8**, 33-55 (1983).

4. G. W. Milliken, E. J. Plautz, R. J. Nudo, Distal forelimb representations in primary motor cortex are redistributed after forelimb restriction: a longitudinal study in adult squirrel monkeys. *J Neurophysiol* **109**, 1268-1282 (2013).

5. D. E. Feldman, M. Brecht, Map plasticity in somatosensory cortex. *Science* **310**, 810-815 (2005).

6. D. S. Bassett, M. S. Gazzaniga, Understanding complexity in the human brain. *Trends Cogn Sci* **15**, 200-209 (2011).

7. M. I. Posner, S. E. Petersen, The attention system of the human brain. *Annu Rev Neurosci* **13**, 25-42 (1990).

8. M. E. Raichle *et al.*, A default mode of brain function. *Proc Natl Acad Sci U S A* **98**, 676-682 (2001).

9. G. L. Shulman, J. M. Ollinger, M. Linenweber, S. E. Petersen, M. Corbetta, Multiple neural correlates of detection in the human brain. *Proc Natl Acad Sci U S A* **98**, 313-318 (2001).

10. B. Biswal, F. Z. Yetkin, V. M. Haughton, J. S. Hyde, Functional connectivity in the motor cortex of resting human brain using echo-planar MRI. *Magn Reson Med* **34**, 537-541 (1995).

11. M. D. Fox *et al.*, The human brain is intrinsically organized into dynamic, anticorrelated functional networks. *Proc Natl Acad Sci U S A* **102**, 9673-9678 (2005).

12. M. D. Greicius, B. Krasnow, A. L. Reiss, V. Menon, Functional connectivity in the resting brain: a network analysis of the default mode hypothesis. *Proc Natl Acad Sci U S A* **100**, 253-258 (2003).

13. B. T. Yeo *et al.*, The organization of the human cerebral cortex estimated by intrinsic functional connectivity. *J Neurophysiol* **106**, 1125-1165 (2011).

14. J. D. Power *et al.*, Functional network organization of the human brain. *Neuron* **72**, 665-678 (2011).

15. D. Cordes *et al.*, Frequencies contributing to functional connectivity in the cerebral cortex in "resting-state" data. *AJNR Am J Neuroradiol* **22**, 1326-1333 (2001).

16. M. J. Lowe, B. J. Mock, J. A. Sorenson, Functional connectivity in single and multislice echoplanar imaging using resting-state fluctuations. *Neuroimage* **7**, 119-132 (1998).

17. M. D. Fox, M. Corbetta, A. Z. Snyder, J. L. Vincent, M. E. Raichle, Spontaneous neuronal activity distinguishes human dorsal and ventral attention systems. *Proc Natl Acad Sci U S A* **103**, 10046-10051 (2006).

18. W. W. Seeley *et al.*, Dissociable intrinsic connectivity networks for salience processing and executive control. *J Neurosci* **27**, 2349-2356 (2007).

19. N. U. Dosenbach, D. A. Fair, A. L. Cohen, B. L. Schlaggar, S. E. Petersen, A dual-networks architecture of top-down control. *Trends Cogn Sci* **12**, 99-105 (2008).

20. S. Marek, N. U. F. Dosenbach, Control networks of the frontal lobes. *Handb Clin Neurol* **163**, 333-347 (2019).

21. N. U. Dosenbach *et al.*, A core system for the implementation of task sets. *Neuron* **50**, 799-812 (2006).

22. E. M. Gordon *et al.*, Precision Functional Mapping of Individual Human Brains. *Neuron* **95**, 791-807 e797 (2017).

23. T. O. Laumann *et al.*, Functional System and Areal Organization of a Highly Sampled Individual Human Brain. *Neuron* **87**, 657-670 (2015).

24. D. Wang *et al.*, Parcellating cortical functional networks in individuals. *Nat Neurosci* **18**, 1853-1860 (2015).

25. S. Mueller *et al.*, Individual variability in functional connectivity architecture of the human brain. *Neuron* **77**, 586-595 (2013).

26. S. Marek *et al.*, Spatial and Temporal Organization of the Individual Human Cerebellum. *Neuron* **100**, 977-993 e977 (2018).

27. D. J. Greene *et al.*, Integrative and Network-Specific Connectivity of the Basal Ganglia and Thalamus Defined in Individuals. *Neuron* **105**, 742-758 e746 (2020).

28. R. M. Braga, R. L. Buckner, Parallel Interdigitated Distributed Networks within the Individual Estimated by Intrinsic Functional Connectivity. *Neuron* **95**, 457-471 e455 (2017).

29. R. A. Poldrack *et al.*, Long-term neural and physiological phenotyping of a single human. *Nat Commun* **6**, 8885 (2015).

30. C. M. Sylvester *et al.*, Individual-specific functional connectivity of the amygdala: A substrate for precision psychiatry. *Proc Natl Acad Sci U S A* **117**, 3808-3818 (2020).

31. D. J. Newbold *et al.*, Plasticity and Spontaneous Activity Pulses in Disused Human Brain Circuits. *Neuron* **107**, 580-589 e586 (2020).

32. J. D. Power, K. A. Barnes, A. Z. Snyder, B. L. Schlaggar, S. E. Petersen, Spurious but systematic correlations in functional connectivity MRI networks arise from subject motion. *Neuroimage* **59**, 2142-2154 (2012).

33. C. Gratton *et al.*, Emergent Functional Network Effects in Parkinson Disease. *Cereb Cortex* **29**, 2509-2523 (2019).

34. M. D. Greicius *et al.*, Resting-state functional connectivity in major depression: abnormally increased contributions from subgenual cingulate cortex and thalamus. *Biol Psychiatry* **62**, 429-437 (2007).

35. A. Kucyi, J. Parvizi, Pupillary dynamics link spontaneous and task-evoked activations recorded directly from human insula. *J Neurosci* 10.1523/JNEUROSCI.0435-20.2020 (2020).

36. T. Harmelech, R. Malach, Neurocognitive biases and the patterns of spontaneous correlations in the human cortex. *Trends Cogn Sci* **17**, 606-615 (2013).

37. B. Guerra-Carrillo, A. P. Mackey, S. A. Bunge, Resting-state fMRI: a window into human brain plasticity. *Neuroscientist* **20**, 522-533 (2014).

38. C. M. Lewis, A. Baldassarre, G. Committeri, G. L. Romani, M. Corbetta, Learning sculpts the spontaneous activity of the resting human brain. *Proc Natl Acad Sci U S A* **106**, 17558-17563 (2009).

39. B. J. Shannon *et al.*, Brain aerobic glycolysis and motor adaptation learning. *Proc Natl Acad Sci U S A* **113**, E3782-3791 (2016).

40. S. E. Petersen, M. I. Posner, The attention system of the human brain: 20 years after. *Annu Rev Neurosci* **35**, 73-89 (2012).

41. M. Neta, S. M. Nelson, S. E. Petersen, Dorsal Anterior Cingulate, Medial Superior Frontal Cortex, and Anterior Insula Show Performance Reporting-Related Late Task Control Signals. *Cereb Cortex* **27**, 2154-2165 (2017).

42. C. L. Wellman, L. L. Arnold, E. E. Garman, P. E. Garraghty, Acute reductions in GABAA receptor binding in layer IV of adult primate somatosensory cortex after peripheral nerve injury. *Brain Res* **954**, 68-72 (2002).

43. E. M. Gordon *et al.*, Three Distinct Sets of Connector Hubs Integrate Human Brain Function. *Cell Rep* **24**, 1687-1695 e1684 (2018).

44. Z. P. Rosenthal *et al.*, Local Perturbations of Cortical Excitability Propagate Differentially Through Large-Scale Functional Networks. *Cereb Cortex* **30**, 3352-3369 (2020).

45. M. Jacomy, T. Venturini, S. Heymann, M. Bastian, ForceAtlas2, a continuous graph layout algorithm for handy network visualization designed for the Gephi software. *PLoS One* **9**, e98679 (2014).

46. E. M. Gordon *et al.*, Generation and Evaluation of a Cortical Area Parcellation from Resting-State Correlations. *Cereb Cortex* **26**, 288-303 (2016).

47. E. M. Gordon *et al.*, Default-mode network streams for coupling to language and control systems. *Proc Natl Acad Sci U S A* **117**, 17308-17319 (2020).

48. B. Fischl, FreeSurfer. *Neuroimage* **62**, 774-781 (2012).

49. D. S. Marcus *et al.*, Informatics and data mining tools and strategies for the human connectome project. *Front Neuroinform* **5**, 4 (2011).

50. J. Bottger, A. Schafer, G. Lohmann, A. Villringer, D. S. Margulies, Three-dimensional mean-shift edge bundling for the visualization of functional connectivity in the brain. *IEEE Trans Vis Comput Graph* **20**, 471-480 (2014).